

1 **Descriptions of four new species of**
2 ***Minyomerus* Horn, 1876 sec. Jansen &**
3 **Franz, 2018 (Coleoptera: Curculionidae),**
4 **with notes on their distribution and**
5 **phylogeny**

6 **M. Andrew Jansen¹ and Nico M. Franz²**

7 **¹School of Life Sciences, 427 E Tyler Mall, PO Box 874501, Tempe, AZ 85287**

8 **²ASU Natural History Collections, 734 W Alameda Dr, Tempe, AZ 85282**

9 Corresponding author:

10 M. Andrew Jansen¹

11 Email address: majanse1@asu.edu

12 **ABSTRACT**

13 This contribution adopts the taxonomic concept approach, including the use of *taxonomic concept labels*
14 (name sec. [*according to*] source) and Region Connection Calculus (RCC–5) articulations and alignments.
15 Prior to this study, the broad-nosed weevil genus *Minyomerus* Horn, 1876 sec. Jansen & Franz, 2015
16 (Curculionidae [non-focal]: Entiminae [non-focal]: Tanymecini [non-focal]) contained 17 species distributed
17 throughout the desert and plains regions of North America. In this revision of *Minyomerus* sec. Jansen &
18 Franz, 2018, we describe the following four species as new to science: *Minyomerus ampullaceus* sec.
19 Jansen & Franz, 2018 (henceforth: [JF2018]), **new species**, *Minyomerus franko* [JF2018], **new species**,
20 *Minyomerus sculptilis* [JF2018], **new species**, and *Minyomerus tylotos* [JF2018], **new species**. The four
21 new species are added to, and integrated with, the preceding revision, and an updated key and phylogeny
22 of *Minyomerus* [JF2018] are presented. A cladistic analysis using 52 morphological characters of 26
23 terminal taxa (5/21 outgroup/ingroup) yielded a single most-parsimonious cladogram (Length = 99 steps,
24 Consistency Index = 60, Retention Index = 80). The analysis reaffirms the monophyly of *Minyomerus*
25 [JF2018] with eight unreversed synapomorphies. The species-group placements, possible biogeographic
26 origins, and natural history of the new species are discussed in detail.

27 **INTRODUCTION**

28 This phylogenetic revision follows Jansen & Franz (2015) in the use of the taxonomic concept approach;
29 see Franz & Peet (2009), Franz et al. (2016a,b). Accordingly:

- 30 1. *Taxonomic concept labels* – i.e., the taxonomic name sec. (*according to*) author or source (year) –
31 are used whenever we identify one specific usage of the taxonomic name. Examples: *Minyomerus*
32 Horn, 1876 sec. Jansen & Franz, 2015 (henceforth: [JF2015]) and *Minyomerus* Horn, 1876
33 sec. Jansen & Franz, 2018 (henceforth: [JF2018]). We also employ this convention to express
34 nomenclatural relationships.
- 35 2. Solely the taxonomic name – without the sec. annotation – is used to refer to the cumulative
36 history (origin to present) of taxonomic concept labels in which that name participates. Example:
37 *Minyomerus* Horn, 1876.
- 38 3. The annotation [non-focal] is added to taxonomic names whose meanings are not under scrutiny in
39 the present context; such as names for higher-level weevil groups and associated plants (exempting
40 common names). Example: Tanymecini Lacordaire, 1863 [non-focal].

41 The weevil genus *Minyomerus* Horn, 1876 [JF2018] remains currently assigned to the tribe Tanymecini
42 Lacordaire, 1863 [non-focal], subtribe Tanymecina Lacoirdaire, 1863 [non-focal] (Curculionidae [non-

43 focal]: Entiminae [non-focal] – higher-level classification in accordance with Alonso-Zarazaga & Lyal
44 1999 and Bouchard et al. 2011). A recent phylogenetic revision of the genus *Minyomerus* [JF2015]
45 recognized a total of 17 described species, distributed throughout the desert and plains regions of North
46 America (Jansen & Franz 2015).

47 Members of the genus *Minyomerus* [JF2018] are phytophagous, and may be found on a variety of
48 host plants, especially the creosote bush *Larrea tridentata* (DC) Coville [non-focal] (Zygophyllaceae
49 [non-focal]), broomweed *Gutierrezia Lagasca* [non-focal] (Asteraceae [non-focal]), sagebrush *Artemisia*
50 Linnaeus [non-focal] (Asteraceae [non-focal]), and occasionally on other various members of Asteraceae
51 [non-focal] (Jansen & Franz 2015). While many species appear to be generalists, the adults are consis-
52 tently observed on the leaves and branches of the host, feeding on the leaf tissue. All other life stages
53 remain unknown. Species of *Minyomerus* [2018] are commonly found in deserts throughout western
54 North America; including the Mojave, Sonoran, Chihuahuan, and Great Basin Deserts. However, their
55 distributional range extends throughout the semi-arid regions of the Great Plains, the Colorado Plateau,
56 and Baja California, México (O'Brien & Wibmer 1982, Jansen & Franz 2015). The adults are flightless,
57 as the hind wings and associated flight structures of all species are either greatly reduced or not readily
58 apparent in dissection.

59 *Minyomerus* [JF2018] belongs to the broad-nosed weevils, subfamily Entiminae [non-focal], on the
60 basis of having a short, broad rostrum and dehiscent mandibular process (Marvaldi 1997, Anderson 2002,
61 Oberprieler et al. 2007, 2014, Marvaldi et al. 2014). The adults are clothed in appressed, circular scales,
62 generally in earth-tones from white to dark brown, with sub-recumbent to erect, interspersed setiform
63 scales ("setae") arranged in rows on the elytral intervals. Their body length can range from 2.8 mm to 6.0
64 mm (Jansen & Franz 2015). The genus has been classified in the tribe Tanymercini [non-focal] based on
65 the presence of post-ocular vibrissae that project anteriorly from the anterior prothoracic margin, although
66 the exact placement and sister taxa of this genus within the tribe are currently unknown (Howden 1959,
67 1970, 1982, Jansen & Franz 2015).

68 *Minyomerus* [JF2015] was circumscribed by a unique combination of synapomorphic traits, described
69 by Jansen & Franz (2015) as follows:

- 70 1. The integument is covered by appressed scales that are sub-circular and overlap posteriorly.
- 71 2. The nasal plate is present as a broad, scale-covered, chevron-shaped ridge demarcating the epistoma.
- 72 3. A sulcus posteriad of nasal plate is present.
- 73 4. The scrobe is sub-equal in length to the funicle and club combined.
- 74 5. The head is directed slightly ventrally.
- 75 6. The metatibial apex lacks setiform bristles yet displays bristles that are shorter to sub-equal in
length to the surrounding setae and conical to lamelliform.
- 76 7. The mesotarsi are slightly shorter than the mesotibiae.
- 77 8. All tarsi lack pads of setiform setae but have stout, spiniform setae.

79 The following additional characters are useful for identifying members of *Minyomerus* [JF2018],
80 especially when differentiating the former from other genera of Tanymercini [non-focal] that may be
81 found together in the same desert habitats; viz. *Isodrusus* Sharp, 1911 [non-focal], *Isodacrys* Sharp, 1911
82 [non-focal], and *Pandeleteinus* Champion, 1911 [non-focal] (see also Anderson 2002):

- 83 1. The intercoxal process of the prosternum is medially divided into two halves, with the procoxae
84 apparently contiguous in most.
- 85 2. The elytral humeri are rounded rather than angled and protruding.
- 86 3. The profemora are not dilated and lack spines.
- 87 4. The protibiae are ventrally excavated by a longitudinal groove or concavity.
- 88 5. A distinct scrobe is present and directed ventrad of the eye, with a more or less apparent tooth
formed by an overhang of the dorsal margin.

90 Following the publication of a monographic revision of *Minyomerus* [JF2015], we have discovered
91 four additional, undescribed species. These are known to us only from limited numbers of specimens, yet
92 are well circumscribed by – i.e., intensionally included in (see Franz & Peet 2009) – the recent generic
93 delimitation of *Minyomerus* [JF2015]. In other words, the addition of these new species *has not* required
94 altering the intensional, property-based definition of the genus-level concept as circumscribed in Jansen

& Franz (2015) (see **Phylogenetic Results**). Our RCC–5 alignments (see **RCC–5 Alignments**) reflect this genus-level concept congruence while also showing which classificatory and phylogenetic structures have changed (Figs. 32–34). The precise use of the taxonomic concept labels in accordance with either [JF2015] or [JF2018] is meant to minimize the creation of new taxonomic concept labels (to counter label “inflation”; see Franz & Peet (2009)), while reflecting explicitly *which* taxonomic concepts we consider as relevantly new and unique to the present study.

Here we describe the four newly found species of *Minyomerus* [JF2018] and provide images of the holotypes and of dissected genitalia for the purpose of identification. We additionally conduct a morphological phylogenetic analysis of the genus to clarify the placement of these new taxa within *Minyomerus* [JF2018], based on the analysis provided in our previous work. An emended identification key to the species of *Minyomerus* [JF2018] is given, along with an updated species checklist. Where possible, we make note of host-plant records, and briefly discuss the geographic distributions of the herein described species. A more extensive discussion of the habits, distribution, and delimitation of the genus *Minyomerus* [JF2015] and all of its constituent species is provided in Jansen & Franz (2015).

MATERIALS AND METHODS

The methods used in this manuscript are generally consistent with Jansen & Franz (2015). Relevant updates are detailed below. In particular, we retain the format for the species descriptions, emphasizing only those characters that vary significantly from the generic circumscription of *Minyomerus* [JF2015].

Acquisition of museum specimens

The set of specimens used in Jansen & Franz (2015) was supplemented with material from the following collections, using the codens of Arnett Jr. et al. (1993):

CMNC Canadian Museum of Nature Collection, Ottawa, Ontario, Canada

TAMU Texas A & M University, College Station, Texas, USA

USNM National Museum of Natural History, Washington, D.C., USA

Georeferencing of localities was performed with Google Earth (Google Inc. 2018), following the WGS 84 standard, and reported in decimal degrees. Taxonomic names for associated host plants, as noted following each species account, are used in accordance with Munz & Keck (1973) and SEINet (2018).

Morphological analysis

Our systematic and descriptive approach is complementary to Jansen & Franz (2015), which in turn follows Franz (2010a,b, 2012). The terminology for exterior morphology is in general accordance with de la Torre-Bueno et al. (1989). Additional morphological terms specific to broad-nosed weevils (Entiminae [non-focal]) were used as follows: Ting (1936) and Morimoto & Kojima (2003) for mouthparts; Thompson (1992) for tibial apices and abdominal segments; and Oberprieler et al. (2014) and Howden (1995) for male and female terminalia.

Measurements were taken with a Leica M205 C stereomicroscope and associated software, Leica Application Suite (LAS), version 4.1.0. Overall body length and width were measured in dorsal view as the maximum distance between the rostral and elytral apices, and the maximum width of both elytra, respectively. Rostral length was measured in dorsal view as the distance between the epistomal apex and the anterior margin of the eyes. Rostral width was measured in dorsal view as the maximum distance between the dorsal margins of the rostrum near the point of antennal insertion. Pronotal length was measured in dorsal view as the length along the midline between the anterior and posterior margins. The width of an individual elytron was measured in dorsal view as the maximum distance between the lateral margin and the elytral suture. Other length and width measurements were also performed in dorsal orientation, using the maximum length and width of the corresponding structure (profemur, protibia, elytron, and aedeagus). Images of mouthparts and terminalia were produced with the Leica microscope equipment, while habitus photographs were created with a Visionary Digital Passport II system using a Canon EOS Mark 5D II camera.

The herein newly recognized species of *Minyomerus* [JF2018] were delimited through application of the phylogenetic species concept *sensu* Wheeler & Platnick (2000). Species descriptions are in alphabetical order, rather than phylogenetic order, for ease of use. As in Jansen & Franz (2015), the

145 species descriptions represent unique, complementary accounts of the character states observed for each
 146 species, including their intra-specific variability, but excepting characters invariant within the genus-level
 147 concept of *Minyomerus* [JF2015]. Likewise, descriptions of males emphasize characters that are variable
 148 and sufficiently different from those of the females to merit recognition. The key to identifying species of
 149 *Minyomerus* [JF2018] is arranged with emphasis being placed on the most readily observable diagnostic
 150 characters. This manuscript is arranged with the species descriptions appearing first, followed by the key
 151 to species, and then by the phylogenetic and RCC–5 alignment results.

152 Phylogenetic analysis

153 The morphological cladistic analysis includes 26 terminal taxa; with 21 ingroup and 5 outgroup terminals.
 154 The ingroup terminals were represented by 17 species previously assigned to *Minyomerus* [JF2015]
 155 and four newly recognized species. In keeping with our previous analysis, we sampled outgroups fairly
 156 broadly while remaining focused on North American lineages that are putative close relatives of the
 157 ingroup (Jansen & Franz 2015, Nixon & Carpenter 1993).

158 Although the tribe Tanymercini [non-focal] is cosmopolitan, the majority of New World species
 159 diversity in the tribe may be found in the subtribe Tanymercina [non-focal] (Alonso-Zarazaga & Lyal
 160 1999). Thus, four of the five outgroup terminals are represented by species belonging to separate genera
 161 in the Tanymercina [non-focal]; viz. *Isodacrys buchanani* Howden, 1961 [non-focal], *Isodrusus debilis*
 162 Sharp, 1911 [non-focal], *Pandeleteinus subcancer* Howden, 1969 [non-focal], and *Pandeleteius cinereus*
 163 (Horn, 1876) [non-focal]. Because generic relationships in the Tanymercini [non-focal] remain unresolved,
 164 we selected a relatively far-removed taxon to root the cladogram that would nevertheless display states
 165 applicable to the ingroup for characters under consideration (Rieppel 2007, Franz 2014). To this end we
 166 used the North American species *Sitona californicus* (Fahraeus, 1840) [non-focal], of the tribe Sitonini
 167 Gistel, 1856 [non-focal].

168 The character matrix was edited and phylogenetic results viewed using the WinDada and WinClados
 169 interfaces of WinClada, respectively (Nixon et al. 2002). The character sequence follows that of the
 170 taxonomic descriptions. The most parsimonious tree and character state optimizations were inferred under
 171 parsimony using NONA (Goloboff 1999). An unconstrained heuristic search was conducted using the
 172 commands: hold 100001, mult*1000, hold/100, with mult*max* selected. Bootstrap support
 173 was inferred in WinClada using the parameters of 1000 replications, hold 1000, hold/100,
 174 mult*10, Don't do max*, and Save consensus. Finally, Bremer support values (Bremer et al.
 175 1994) and relative fit difference (Goloboff & Farris 2001) were calculated in NONA using the commands:
 176 hold 1001, sub 20, bs for Bremer support values, and bs* for relative fit difference, respectively
 177 (Goloboff et al. 2008).

The motivation for providing Bremer support values and relative fit difference comes from their respective interpretations, based on how the measures are calculated, *per* Goloboff & Farris (2001). Both of these indices rely on summation of the number of favorable and contradictory characters when comparing a most-parsimonious tree to a suboptimal tree. If the step length of the i^{th} character (I) of n total characters on the most-parsimonious tree (L_{MPT}) is less than its corresponding step length on the suboptimal tree (L_{SUB}), the character is designated as favorable (f_i), but if the opposite is true, the character is designated as contradictory (c_i), and expressed formally:

$$I = \begin{cases} f_i & L_{MPT} < L_{SUB} \\ c_i & L_{MPT} > L_{SUB} \end{cases} \quad (1)$$

Where the number of favorable (F) and contradictory (C) characters are defined, respectively, as:

$$F = \sum_{n=0}^i f_i \quad (2)$$

$$C = \sum_{n=0}^i c_i \quad (3)$$

Bremer support values (bsv) and relative fit difference (rfd) are then calculated simply as:

$$\text{bsv} = F - C \quad (4)$$

$$\text{rfd} = \frac{F - C}{F} \times 100 \quad (5)$$

178 The Bremer support value for a node thus indicates how many more characters support a node than
179 contradict it, while the relative fit difference indicates what proportion of the favorable characters are
180 represented by the Bremer support value. Whereas the Bremer support value is as large as the number
181 of characters supporting the node, in excess of the contradicting characters, the relative fit difference
182 can only vary from 0 to 100, as a proportion of the number of supporting characters. By providing both
183 measures, one may quickly discriminate, for example, between a node supported by 4 characters but
184 contradicted by 1 character ($bsv = 3$, $rfd = 75$), and a node supported by 10 characters but contradicted by
185 7 characters ($bsv = 3$, $rfd = 30$).

186 **Taxonomic annotations and RCC–5**

187 In accordance with Jansen & Franz (2015), we use the symbol “=” to indicate nomenclatural synonymy
188 (objective/subjective); and the RCC–5 symbols {==, >, <, ><, !} indicate taxonomic concept articula-
189 tions. The annotations (INT) and (OST) indicate intensional and ostensive readings of articulations, and
190 AND is used to connect multiple simultaneously recognized provenance relationships. Two *intensional*
191 alignments are produced as part of this revision, i.e., one that captures the non-/congruence of *Minyomerus*
192 [JF2018] versus *Minyomerus* [JF2015] represented as rank-only classifications (Fig. 32), and another
193 that represents these as fully bifurcated phylogenies with newly assigned clade concept labels, shown in
194 whole-concept resolution (Fig. 33) and in split-concept resolution (Fig. 34); see Franz et al. (2018).

195 A detailed breakdown of our alignment approach and outcomes using an RCC–5 logic reasoner toolkit
196 (Chen et al. 2014) is provided in the **Supplemental Information, SII to SI4**. For further information,
197 see also Jansen & Franz (2015), Franz et al. (2016a,b).

198 **Species distribution modeling**

199 We used the modeling program Maxent, Version 3.4, to generate habitat models for the species of
200 *Minyomerus* [JF2018] (Figs. 35–38) based on documented occurrence records (Phillips et al. 2004, 2006,
201 Elith et al. 2011). The default settings were adjusted to Max number background points =
202 100,000 and Iterations = 10. Cross-validation was used to leverage all available locality data;
203 however, no models could be created for species with two or fewer documented localities. We selected
204 19 bioclimatic variables and elevation as Environmental Layers in Maxent, obtained from WorldClim
205 (Hijmans et al. 2005). The layers were downloaded by tile (zones 11–13 and 21–23), with a 30 arc-second
206 resolution (projected using WSG 84) to provide adequate coverage of the full distribution of the genus.
207 Layerwise assembly of tiles was done using QGIS, Version 2.18.16 ‘Las Palmas’, creating composite
208 maps of six tiles each to use in species distribution modeling (Quantum GIS Development Team 2018).

209 The rasterized predictive probabilities were imported into QGIS, where each file was designated a
210 specific color. Each pixel in the raster was assigned a linearly interpolated saturation of that color, with
211 increasing saturation denoting an increased probability of successful prediction of species presence at that
212 point. Pixels with a value below 0.50 were rendered transparent so that the maps only show regions with
213 a greater than 50% chance of successful prediction. The raster files were clipped to remove extraneous
214 predicted regions based on: (1) predictive probability (i.e., removing large areas with only transparent
215 pixels) and (2) geographic extent (accounting for endemism). For example, a species endemic to the
216 Snake River Valley of Idaho does not require a predictive model for bioclimatically similar habitats in the
217 Chihuahuan Desert. Documented occurrence records are laid over the modeled habitat ranges as colored
218 circles on their respective maps (Figs. 36–38), along with vector layers of country (white) and state (gray)
219 borders (Hijmans et al. 2012).

220 **Nomenclature**

221 The electronic version of this article in Portable Document Format (PDF) will represent a published work
222 according to the International Commission on Zoological Nomenclature (ICZN), and hence the new names
223 contained in the electronic version are effectively published under that Code from the electronic edition
224 alone. This published work and the nomenclatural acts it contains have been registered in ZooBank, the
225 online registration system for the ICZN. The ZooBank LSIDs (Life Science Identifiers) can be resolved
226 and the associated information viewed through any standard web browser by appending the LSID to
227 the prefix <http://zoobank.org/>. The LSID for this publication is: urn:lsid:zoobank.org:pub:0AEE5733-
228 06D1-401F-88C9-0D5232FBFC7A. The online version of this work is archived and available from the
229 following digital repositories: PeerJ, PubMed Central and CLOCKSS.

230 *Minyomerus ampullaceus*: *Minyomerus franko*: *Minyomerus sculptilis*: *Minyomerus tylotos*:

231 **DESCRIPTIONS OF NEW SPECIES**

232 ***Minyomerus ampullaceus* Jansen & Franz sec. Jansen & Franz, 2018; sp. n.**

233 urn:lsid:zoobank.org:act:24943E17-F20E-4E3C-A3A1-A1D4D907B48E

234 Figures 1-6

235 **Diagnosis**

236 *Minyomerus ampullaceus* [JF2018] is best differentiated from other congeners by its unique body shape,
237 which most prominently features a strongly constricted, sub-cylindrical pronotum and greatly protuberant
238 elytra; this combination gives the species a distinctly flask- or bottle-shaped appearance. Due to the
239 relatively poor condition of the scales and setae of the holotype, color and setation cannot be reliably
240 used for identification. However, the elytra themselves are unique in shape, and diagnostic, together
241 nearly 2× the width of the pronotum at their widest point, and nearly 3/4× as wide as long in dorsal
242 view. In lateral view the anterior and posterior declivities of the elytra are strongly abrupt, and nearly
243 vertical; most notably, the anterior margin of the elytra projects strongly and characteristically dorsad of
244 its articulation with the posterior pronotal margin. The spermatheca is also quite distinct, having a highly
245 elongate projection of the corpus aligned with midline of the ramus, which is basally tapered and angled
246 at nearly 45° to the corpus.

247 **Description of female**

248 **Habitus** Length 3.76 mm, width 1.76 mm, length/width ratio 2.14, widest at anterior 1/3 of elytra.
249 Integument orange-brown to black. Scales with variously interspersed colors ranging from slightly
250 off-white to beige to yellow. Setae recumbent to sub-recumbent, white to brown in color.

251 **Mandibles** Partially covered with white, slightly opalescent scales, with 3 longer setae, and 1 shorter
252 seta between these.

253 **Rostrum** Length 0.54 mm, anterior portion 1.5-2× broader than long, rostrum/pronotum length ratio
254 0.57, rostrum length/width ratio 1.10. Separation of rostrum from head generally obscure. Dorsal outline
255 of rostrum nearly square, anterior half of dorsal surface mesally concave, posterior half coarsely but
256 shallowly punctate to rugose. Rostrum in lateral view nearly square; apical margin broadly bisinuate and
257 emarginate, with 2 pairs of large vibrissae. Nasal plate defined by Y-shaped, impressed lines, convex,
258 integument partially covered with white scales. Margins of mandibular incision directed ca. 15° outward
259 dorsally in frontal view. Ventrolateral sulci strongly defined, beginning as a narrow sulcus posteriad of
260 insertion point of mandibles, running parallel to scrobe, terminating in a ventral fovea.

261 **Antennae** Small tooth formed by overhanging dorsal margin of scrobe directly ventrad of margin of
262 eye. Scape extending to posterior 1/3 of eye. Funicular segments V-VII and club missing.

263 **Head** Eyes globular, anterodorsal margin of each eye feebly impressed, posterior margin elevated
264 from lateral surface of head; eyes separated in dorsal view by 4× their anterior-posterior length, set off
265 from anterior prothoracic margin by 1/3 of their anterior-posterior length. Head without any transverse
266 post-ocular impression.

267 **Pronotum** Length/width ratio 0.88; widest near midpoint. Anterior margin slightly arcuate, lateral
268 margins curved and widening into a bulge just anteriad of midpoint of pronotum, posterior margin straight,
269 with a slight mesal incurvature. Pronotum in lateral view with setae that reach beyond anterior margin by
270 1/2 of their length; these setae becoming evenly longer and more erect laterally, reaching a maximum
271 length equal to 1/2 of length of eye. Anterolateral margin with a reduced tuft of 6-7 post-ocular vibrissae
272 present, emerging near ventral 1/2 of eye, and stopping just below ventral margin of eye; vibrissae sub-
273 equal in length at 1/3 of anterior-posterior length of eye, except for three vibrissae achieving a maximum
274 length similar to anterior-posterior length of eye.

275 **Scutellum** Exposed, margins straight.

276 **Pleurites** Metepisternum hidden by elytron.

277 **Thoracic sterna** Mesocoxal cavities separated by 1/4× width of mesocoxal cavity. Metasternum with
278 transverse sulcus not apparent; metacoxal cavities widely separated by ca. 2× their width.

279 **Legs** Profemur/pronotum length ratio 1.04; profemur with distal 1/5 produced ventrally as a rounded
280 projection covering tibial joint; condyle of tibial articulation occupying 4/5 of distal surface and 1/5
281 length of femur. Protibia/profemur length ratio 0.93; protibial apex with ventral setal comb recessed in
282 an incurved groove; mucro present as a large, black, sub-triangular, medially-projected tooth, which is
283 approximately equilateral and whose sides are sub-equal in length to surrounding setae. Protarsus with
284 tarsomere III 1.25× as long as II; wider than long. Metatibial apex with almond shaped convexity ringed
285 by 10 short, spiniform setae.

286 **Elytra** Length/width ratio 2.66; widest at anterior 1/3; anterior margins jointly almost 2× wider than
287 posterior margin of pronotum and strongly produced dorsally from margin of pronotum; lateral margins
288 evenly rounded until posterior 1/3, more strongly rounded and converging thereafter. Posterior declivity
289 angled at nearly 85° to main body axis. Elytra with 10 complete striae; striae shallow; punctures faint
290 beneath appressed scales, separated by 5–7× their diameter; intervals very slightly elevated.

291 **Abdominal sterna** Ventrite III anteromesally incurved around a fovea located mesally on anterior
292 margin, posterior margin elevated and set off from IV along lateral 1/3s of its length. Sternum VII mesally
293 1/2× as long as wide; anterior margin weakly curved.

294 **Tergum** Pygidium (tergum VIII) sub-conical; posterior margin emarginate; medial 1/3 of anterior 3/5
295 of pygidium less sclerotized.

296 **Sternum VIII** Anterior laminar edges each incurved forming a 115° angle with lateral margin, this angle
297 distinctly sclerotized; posterior 1/2 of lamina porose throughout, laminar arms more sclerotized medially;
298 posterior edge evenly, moderately arcuate.

299 **Ovipositor** Coxites in dorsal view slightly longer than broad, with a medial region that is weakly
300 sclerotized.

301 **Spermatheca** Comma-shaped; collum expanded to form a long, cylindrical projection, sub-equal in
302 length to ramus, 1/3× width of corpus, angled at 45° to corpus, apically with a reduced hood-shaped
303 projection; ramus elongate, bulbous, slightly wider than thickness of corpus, basally constricted to form a
304 short stalk; corpus not greatly swollen; cornu sub-equal in length to corpus and collum, recurved distally
305 to form an inner angle of 60° to corpus, straight and gradually narrowing along basal 2/3, with apical 1/3
306 abruptly narrowed, angled at 45° to corpus, and tapering to a slight knob.

307 **Description of male**

308 Male not available or known.

309 **Comments**

310 Due to the limited number of specimens of this species, dissections of mouthparts could not be performed.

311 **Etymology**

312 Named in reference to the shape of the body in dorsal view, which appears bottle-shaped due to the large
313 elytra and comparatively cylindrical pronotum – *ampullaceus* = "flasklike"; Latin adjective (Brown 1956).

314 **Material examined**

315 **Holotype** ♀ "Carlsbad, N.M.; Geococcyx calif; 144640" (**USNM**).

316 **Distribution**

317 This species is known only from Carlsbad, New Mexico (USA), from an unspecified locality; the location
318 of the city is shown in Fig. 36.

319 **Natural history**

320 No host plant associations have been documented. The label indicates "Geococcyx calif"; this is
321 presumably a reference to *Geococcyx californianus* (Lesson, 1829) [non-focal] (Cuculidae [non-focal]),
322 the Greater Roadrunner, although it is unclear if the specimen was found on or near one of these birds
323 (either living, dead, or in a nest). Species of *Minyomerus* [JF2018] are only known to be phytophagous,
324 not parasitic, phoretic, or necrophagous. Hence we believe that this specimen was most likely found in a
325 nest, and was present there only incidentally because the nest was constructed in the host plant of this
326 specimen (Jansen & Franz 2015). It is unknown whether this species is parthenogenetic.

327 ***Minyomerus franko* Jansen & Franz sec. Jansen & Franz, 2018; sp. n.**
328 urn:lsid:zoobank.org:act:F8C0153E-DF0E-40E0-AF31-EBEA7075D06D
329 Figures 7-15

330 **Diagnosis**

331 *Minyomerus franko* [JF2018] is readily distinguished from other congeners by the strikingly long setae
332 of the anterior margin of the pronotum, which project laterally up to 80° from the longitudinal axis of
333 the body and achieve a maximum length at least equaling the diameter of the eye. In addition, the setae
334 lining the dorsal margin of the ocular impression are elongate and reach a length equal to 1/2 - 3/4× the
335 diameter of the eye. The spermatheca has a short, somewhat bulbous corpus, with the ramus sub-equal
336 in size and perpendicular to the corpus, and the collum is strongly recurved along the basal 1/3 of its
337 length. The aedeagus is relatively short and wide, and is abruptly constricted in the apical 1/5 of its length,
338 thereafter tapered to a rounded point.

339 **Description of female**

340 **Habitus** Length 3.10-3.30 mm, width 1.38-1.44 mm, length/width ratio 2.25-2.29, widest at anterior
341 1/3-1/4 of elytra. Integument orange-brown to black. Scales with variously interspersed colors ranging
342 from slightly off-white or beige to manila/tan to dark coffee brown, in some specimens appearing semi-
343 translucent (in others opaque). Setae linear to slightly apically explanate, appearing minutely spatulate,
344 sub-recumbent to sub-erect, white or brown in color.

345 **Mandibles** Covered with white scales, with 3 longer setae, and 1-2 shorter setae between these.

346 **Maxillae** Cardo bifurcate at base with an inner angle typically between 90–120°, arms of equal length,
347 inner (mesal) arm nearly 1.5× thicker than outer arm, both arms of bifurcation equal in length to apically
348 outcurved arm, glabrous. Stipes sub-quadrata, roughly equal in length to each bifurcation of cardo, with a
349 single lateral seta. Galeo-lacinial complex nearly extending to apex of maxillary palpomere II; complex
350 mesally membranous, laterally sclerotized, with sharp demarcation of sclerotized region separating
351 palpiger from galeo-lacinial complex; setose in membranous area just adjacent to sclerotized region, setae
352 covering 2/3 of dorsal surface area; dorsally with 7 apicomesal lacinial teeth; ventrally with 4 reduced
353 lacinial teeth. Palpiger with a single lateral seta, otherwise glabrous and evenly sclerotized throughout.

354 **Maxillary palps** I apically oblique, apical end forming a 45° angle with base, with 2 apical setae; II
355 sub-cylindrical, with 1 apical seta.

356 **Labium** Prementum roughly trapezoidal; apical margins angulate, ventral margin gently sinuate, dorsal
357 margin straight; lateral margins feebly incurved near posterior margin; basal margin arcuate. Labial palps
358 3-segmented, I with apical 2/3 projecting beyond margin of prementum, exceeding apex of ligula; III
359 slightly longer than II.

360 **Rostrum** Length 0.46-0.48 mm, anterior portion 1.75-2.25× broader than long, rostrum/pronotum
361 length ratio 0.58-0.59, rostrum length/width ratio 1.21-1.26. Separation of rostrum from head generally
362 obscure. Dorsal outline of rostrum sub-rectangular, anterior half of dorsal surface feebly impressed,
363 posterior half coarsely but shallowly punctate to rugose. Rostrum in lateral view nearly square; apical
364 margin bisinuate and emarginate, with 2 large vibrissae. Nasal plate defined by broad, V-shaped, shallowly
365 impressed lines, anteromesally slightly convex, integument partially covered with white scales. Margins
366 of mandibular incision directed ca. 15° outward dorsally in frontal view. Ventrolateral sulci weakly
367 defined (or entirely absent in some specimens) as a broad concavity dorsad of insertion point of mandibles,
368 running parallel to scrobe, becoming flatter posteriorly and disappearing ventrally. Dorsal surface of
369 rostrum with short, linear, median fovea. Rostrum ventrally lacking sulci at corners of oral cavity.

370 **Antennae** Small tooth formed by overhanging dorsal margin of scrobe anterior to margin of eye by 1/5
371 of length of eye. Scape nearly extending to posterior 1/4 of eye. Terminal funicular antennomere lacking
372 appressed scales, having instead a covering of apically-directed pubescence with interspersed sub-erect
373 setae. Club nearly 3× as long as wide.

374 **Head** Eyes globular to slightly elongate, slanted ca. 35° antero-ventrally; eyes separated in dorsal
375 view by 4× their anterior-posterior length, set off from anterior prothoracic margin by 1/3 of their
376 anterior-posterior length. Head without any transverse post-ocular impression.

377 **Pronotum** Length/width ratio 0.84-0.86; widest near anterior 1/3, between anterior constriction and
378 midpoint. Anterior margin arcuate, lateral margins curved and widening into a slight bulge just anteriad
379 of midpoint of pronotum, posterior margin straight, with a slight mesal incurvature. Pronotum in lateral
380 view with setae that reach just beyond anterior margin, angled laterally at 45-80° to longitudinal axis, and
381 strikingly long; these setae becoming evenly longer and more angled laterally, reaching a maximum length
382 nearly equal to length of eye. Anterolateral margin with a reduced tuft of 5 post-ocular vibrissae present,
383 emerging near ventral 1/2 of eye, and stopping just below ventral margin of eye; vibrissae sub-equal
384 in length at 1/3× anterior-posterior length of eye, except for one vibrissa achieving a maximum length
385 similar to anterior-posterior length of eye.

386 **Scutellum** Narrowly exposed, with visible area approximately equal to length of appressed scales,
387 margins straight.

388 **Pleurites** Metepisternum nearly hidden by elytron except for triangular extension.

389 **Thoracic sterna** Mesocoxal cavities separated by 1/3× width of mesocoxal cavity. Metasternum with
390 transverse sulcus not apparent; metacoxal cavities widely separated by ca. 2× their width.

391 **Legs** Profemur/pronotum length ratio 1.01-1.02; profemur with distal 1/5 produced ventrally as a sub-
392 rectangular projection covering tibial joint; condyle of tibial articulation occupying 4/5 of distal surface
393 and 1/5 length of femur. Protibia/profemur length ratio 0.86-0.89; protibial apex with ventral setal comb
394 recessed in a subtly incurved groove; mucro present as a large, black, sub-triangular, medially-projected
395 tooth, which is approximately equilateral and whose sides are sub-equal in length to surrounding setae.
396 Protarsus with tarsomere III 2× as long as II; wider than long. Metatibial apex with almond shaped
397 convexity ringed by 8-9 short, spiniform setae.

398 **Elytra** Length/width ratio 3.08-3.20; widest at anterior 1/3-1/4; anterior margins jointly 1.5× wider than
399 posterior margin of pronotum; lateral margins sub-parallel to slightly rounded after anterior 1/3, more
400 strongly rounded and converging in posterior 1/3. Posterior declivity angled at 70-85° to main body axis.
401 Elytra with 10 complete striae; striae shallow; punctures faint beneath appressed scales, separated by
402 5-7× their diameter; intervals very slightly elevated.

403 **Abdominal sterna** Ventrite III anteromesally incurved around a fovea located mesally on anterior
404 margin, posterior margin elevated and set off from IV along lateral 1/3s of its length. Sternum VII mesally
405 1/2× as long as wide; setae darkening, lengthening, and becoming more erect in posterior 2/3; anterior
406 margin weakly curved.

407 **Tergum** Pygidium (tergum VIII) sub-cylindrical; medial 1/3 of anterior 2/3 of pygidium less sclerotized.

408 **Sternum VIII** Anterior laminar edges each incurved forming a 140° angle with lateral margin; slightly
409 less sclerotized medially between arms of bifurcation; posterior edge subtly incurved medially.

410 **Ovipositor** Coxites 1.5× as long as broad, glabrous; styli 1/2× as long as coxites. Genital chamber
411 apically sclerotized.

412 **Spermatheca** Comma-shaped; collum short, apically with a large, hood-shaped projection angled
413 at ca. 60° to ramus, nearly equal in length and contiously aligned with curvature of bulb of ramus;
414 collum sub-contiguous with, and angled at 90° to ramus; ramus elongate, sub-cylindrical to slightly
415 bulbous, 4/5× thickness of corpus; corpus swollen, 1.25× thickness of ramus and 1.5× thickness of cornu;
416 cornu elongate, strongly recurved in basal 1/3, nearly straight thereafter and narrowing apically, abruptly
417 narrowed in apical 1/3 with apex angled at 30° to corpus.

418 **Description of male**

419 Similar to female, except where noted.

420 **Habitus** Length 2.47-2.81 mm, width 0.99-1.24 mm, length/width ratio 2.27-2.49. Rostrum length
421 0.30-0.42 mm, rostrum/pronotum length ratio 0.44-0.53, rostrum length/width ratio 1.00-1.08. Pronotum
422 length/width ratio 0.91-1.00. Profemur/pronotum length ratio 0.87-0.90, protibia/profemur length ratio
423 0.87-0.97. Elytra length/width ratio 3.00-3.10.

424 **Elytra** Elytral declivity more angulate than female on average, forming an 80° angle to main body axis,
425 but otherwise as in female.

426 **Abdominal sterna** Sternum VII 2/5-1/2× as long as wide, posterior margin arcuate mesally.

427 **Tergum** Pygidium (tergum VIII) with posterior 1/3 punctate; anterior 2/3 rugose.

428 **Sternum IX** Spiculum gastrale 2× length of aedeagal pedon. Laminar alae located on lateral 1/4 of
429 posterior margin.

430 **Aedeagus** Length/width ratio 2.78-3.16; lateral margins very slightly converging posteriorly, abruptly
431 constricted and more strongly converging in apical 1/5. Pedon in lateral view becoming gradually narrower
432 posteriorly in anterior 1/2, ventral margins in posterior 1/2 abruptly curving to meet dorsal margins at a
433 rounded apical point. Flagellum with large, elongate, tortuous apical sclerite, sclerite nearly as long as
434 pedon, with complex, asymmetrical interior structure.

435 **Etymology**

436 Named in reference to the long, somewhat unkempt, erect setae on the anterior margin of the pronotum—
437 *franko* = “free”; Old High-German adjective (Brown 1956).

438 **Material examined**

439 **Holotype** ♀ “MEX: S.L.P 1 km N.; Entronque El Huizache; 1493 m 2.VI.87; R. Anderson, *Sphaeralcea*;
440 *hastula* A. Gray” [non-focal] (**CMNC**).

441 **Paratypes** Same label information as female holotype (**CMNC**: 1 ♀, 1 ♂; **TAMU**: 2 ♂); “MEXICO:
442 S.L.P; 19.6 mi. n. Huizache; July 25, 1976; Peigler, Gruetzmacher, R&M Murray, Schaffner” (**CMNC**: 1
443 ♂); “MEXICO: San Luis Potosí; Entronque el Hulzache; 2 June 1987; R. Turnbow” (**CMNC**: 1 ♀, 1 ♂);
444 “MEXICO: Tamaulipas; 8.8 mi. ne. Jaumave; October 10, 1973; Gaumer & Clark” (**TAMU**: 2♀); “9 mi
445 east Santo Domingo, S.L.P.; Mexico XI-14-68; Veryl V. Board” (**TAMU**: 2 ♂).

446 **Distribution**

447 This species has been found in San Luis Potosí and Tamaulipas (Mexico). It is likely to be found
448 throughout the Chihuahuan Desert and arid regions of south-central Mexico based on habitat similarity
449 (Fig. 37).

450 **Natural history**

451 Associated with spear globemallow *Sphaeralcea hastulata* A. Gray [non-focal] (Malvaceae [non-focal]).

452 ***Minyomerus sculptilis* Jansen & Franz sec. Jansen & Franz, 2018; sp. n.**

453 urn:lsid:zoobank.org:act:EA0B1AD9-68F2-4409-A0F8-903B0DA0FFF9

454 Figures 16-22

455 **Diagnosis**

456 *Minyomerus sculptilis* [JF2018] is best distinguished from other congeners, especially *Minyomerus*
457 *imberbus* Jansen & Franz, 2015 [JF2015], by a combination of characters, as follows. The interspersed
458 setae on the body are linear and either brown or white. The anterior margin of the pronotum bears a
459 reduced tuft of post-ocular vibrissae. The head is barely elevated between the eyes. The ventrolateral
460 sulci of the rostrum are well defined. The lateral face of each elytron has the intervals raised and well
461 sculpted in appearance. The spermatheca is distinct and has an elongate, annulate, basally tapered ramus,
462 which is slightly thinner than corpus. The cornu is strongly recurved in the basal half, giving it a uniquely
463 sinuate appearance. Both the corpus and cornu terminate in large, hood-shaped, explanate projections
464 equal in size to the ramus. The aedeagus is elongate, acutely angulate, and narrowing towards the apex
465 more strongly in the region of the ostium.

466 **Description of female**

467 **Habitus** Length 3.39-3.70 mm, width 1.33-1.58 mm, length/width ratio 2.34-2.55, widest at anterior
468 1/5 of elytra. Integument orange-brown to black. Scales with variously interspersed colors ranging from
469 slightly off-white or beige to golden brown to dark coffee brown. Setae sub-recumbent to sub-erect, white
470 to brown in color.

471 **Mandibles** Covered with white scales, with 3 longer setae, and 1 shorter seta between these.

472 **Rostrum** Length 0.50-0.59 mm, anterior portion ca. 1.5× broader than long, rostrum/pronotum length
473 ratio 0.66-0.67, rostrum length/width ratio 1.43-1.48. Separation of rostrum from head generally obscure.
474 Dorsal outline of rostrum nearly square, anterior half of dorsal surface mesally concave, posterior half
475 coarsely but shallowly punctate to rugose. Rostrum in lateral view nearly square; apical margin bisinuate
476 and emarginate, with 2 pairs of large vibrissae. Nasal plate defined by Y-shaped, impressed lines, convex,
477 integument covered with white scales. Margins of mandibular incision directed ca. 15-20° outward
478 dorsally in frontal view. Ventrolateral sulci strongly defined, beginning as a narrow sulcus posteriad of
479 insertion point of mandibles, running parallel to scrobe, terminating in a ventral fovea.

480 **Antennae** Dorsal margin of scrobe overhanging broadly (not forming a minute tooth). Funicle slightly
481 longer than scape. Scape extending Brassicaceae to posterior 1/4 of eye. Club nearly 3× as long as wide.

482 **Head** Eyes globular, anterodorsal margin of each eye impressed, posterior margin slightly elevated
483 from lateral surface of head; eyes separated in dorsal view by 5× their anterior-posterior length, set off
484 from anterior prothoracic margin by 1/4 of their anterior-posterior length. Head between eyes rugose and
485 slightly bulging.

486 **Pronotum** Length/width ratio 0.85-0.87; widest near anterior 2/5. Anterior margin arcuate, subtly
487 incurved mesally, and somewhat produced dorsally; anterior constriction broad, posterior margin slightly
488 arcuate. Pronotum in lateral view with setae that reach beyond anterior margin; these setae becoming
489 slightly longer and more erect laterally. Anterolateral margin with a reduced tuft of 3-6 post-ocular
490 vibrissae present, emerging near ventral 1/2 of eye, and stopping just below ventral margin of eye;
491 vibrissae varying in length from 1/2× anterior-posterior length of eye to a maximum length similar to
492 anterior-posterior length of eye.

493 **Scutellum** Exposed, margins straight.

494 **Pleurites** Metepisternum nearly hidden by elytron except for triangular extension.

495 **Thoracic sterna** Mesocoxal cavities separated by 1/3× width of mesocoxal cavity. Metasternum with
496 transverse sulcus not apparent; metacoxal cavities widely separated by ca. 2× their width.

497 **Legs** Profemur/pronotum length ratio 0.92-1.03; profemur with distal 1/6 produced ventrally as a
498 slightly rounded, sub-rectangular projection covering tibial joint; condyle of tibial articulation occupying
499 4/5 of distal surface and 1/6 length of femur. Protibia/profemur length ratio 0.87-0.93; protibial apex with
500 ventral setal comb recessed in a subtly incurved groove; mucro not apparent. Protarsus with tarsomere III
501 1.5× as long as II; wider than long. Metatibial apex with almond shaped convexity ringed by 10-12 short,
502 spiniform setae.

503 **Elytra** Length/width ratio 3.12-3.16; widest at anterior 1/5; anterior margins jointly 1.5-2× wider
504 than posterior margin of pronotum; lateral margins gently converging after anterior 1/5, more strongly
505 converging in posterior 1/4. Posterior declivity angled at 65-70° to main body axis. Elytra with 10
506 complete striae; striae broadly sculpted; punctures faint beneath appressed scales, separated by 5-7× their
507 diameter; intervals elevated, with every second interval, beginning at elytral suture, more strongly raised
508 than adjacent intervals.

509 **Abdominal sterna** Ventrite III anteromesally incurved around a fovea located mesally on anterior
510 margin, posterior margin elevated and set off from IV along lateral 1/3s of its length. Sternite VII mesally
511 2/3× as long as wide; anterior margin straight.

512 **Tergum** Pygidium sub-cylindrical; medial 1/2 of anterior 3/5 of pygidium less sclerotized.

513 **Sternum VIII** Anterior laminar edges of spiculum ventrale each incurved forming a 125° angle with
514 lateral margin; lamina more sclerotized medially; posterior margin medially incurved.

515 **Ovipositor** Coxites as long as broad; styli as long as coxites, glabrous.

516 **Spermatheca** S-shaped; collum short, apically with a large, hood-shaped projection roughly aligned
517 with central axis of corpus, nearly equal in length to bulb of ramus; collum sub-contiguous with, and
518 angled at 30° to ramus; ramus elongate, sub-cylindrical to slightly bulbous, 3/4× thickness of corpus,
519 with a short stalk oriented at ca. 45° to the corpus; corpus swollen, 1.3× thickness of ramus; cornu short,

520 2.5-3× length or ramus, recurved and strongly arched in basal 1/2, forming an inner angle of ca. 80° ,
521 feebly sinuate thereafter, with apical 1/2 expanded, then abruptly constricted near apical 1/4 to a fine
522 point.

523 **Description of male**

524 Similar to female, except where noted.

525 **Habitus** Length 3.10 mm, width 1.22 mm, length/width ratio 2.54. Rostrum length 0.53 mm, rostrum/pronotum length ratio 0.65, rostrum length/width ratio 1.66. Pronotum length/width ratio 0.99.
526 Profemur/pronotum length ratio 1.01, protibia/profemur length ratio 0.82. Elytra length/width ratio 3.18.
527

528 **Elytra** Elytral declivity slightly less angulate than female, forming a 60° angle to main body axis, but
529 otherwise as in female.

530 **Abdominal sterna** S sternum VII 1/2× as long as wide, posterior margin feebly arcuate mesally.

531 **Tergum** Pygidium (tergum VIII) with mesal 1/3 of posterior margin subtly incurved; posterior 2/3
532 punctate; anterior 1/3 rugose.

533 **Sternum VIII** Consisting of 2 sub-triangular sclerites; antero-laterally with a sharply-pointed projection
534 as long as anterior-posterior length of triangular portion of sclerite.

535 **Aedeagus** Length/width ratio 7.00; lateral margins parallel, more strongly converging in region of
536 ostium. In lateral view, width of pedon even throughout in anterior 2/3, ventral margins in posterior 1/3
537 becoming straight towards apex, then curving to meet dorsal margins at a sharp apical point; apex acutely
538 angulate. Flagellum without apparent sclerite.

539 **Comments**

540 Due to the limited number of specimens of this species, dissections of mouthparts could not be performed.

541 **Etymology**

542 Named in reference to the elevated elytral intervals, which give this species a sculpted appearance –
543 *sculptilis* = "sculpted"; Latin adjective (Brown 1956).

544 **Material examined**

545 **Holotype** ♀ "Burley, Idaho; #7, 5-20-32; *A.[rtemisia] tridentata* [non-focal]; David E. Fox" (**USNM**).

546 **Paratypes** "Milner, Idaho; #5a, 7-9-31; *S.[alsola] pestifer*; David E. Fox" (**USNM**: 1 ♀); "Hazelton, Ida;
547 #10 4/29/30; *N.[orta] altissima*" (**USNM**: 1 ♂)

548 **Distribution**

549 This species has been found in three localities along the Snake River in Idaho (USA), and is thought to be
550 endemic to the Snake River Plain (Fig. 38).

551 **Natural history**

552 Associated with big sagebrush *Artemisia tridentata* Nutt. [non-focal] (Asteraceae [non-focal]), tumble-
553 weed *Salsola tragus* L. [non-focal] (= *Salsola pestifer* A. Nelson [non-focal]) (Amaranthaceae [non-focal]),
554 and tall tumblemustard *Sisymbrium altissimum* L. [non-focal] (= *Norta altissima* (L.) Britt. [non-focal])
555 (Brassicaceae [non-focal]).

556 **Minyomerus tylotos Jansen & Franz sec. Jansen & Franz, 2018; sp. n.**

557 urn:lsid:zoobank.org:act:10CD3562-5969-4BCF-ACFE-BB0E5E2BF9A6

558 Figures 23-29

559 **Diagnosis**

560 *Minyomerus tylotos* [JF2018] is most readily distinguished from other congeners by a combination
561 of characters, as follows. The nasal plate lacks distinct impressions, having instead a poorly defined
562 anteromesal convexity completely and evenly covered with white scales. The frons is protuberant and
563 moderately punctate. The entire body, including the legs, head, and venter, are clothed with brown,
564 linear to minutely apically expanded setae, which are of similar length throughout and appear distinctly
565 undifferentiated and uniform across body regions. The body is somewhat bulky, with the pronotum

566 protuberant laterally and globular in dorsal view. The setae lining the anterodorsal margin of the pronotum
567 uniquely apically explanate, with a longitudinal, medial, ridge-like portion that tapers to either side
568 apicolaterally (visible at high magnification). The lateral margins of the elytra are protuberant anteriorly
569 and sub-parallel along the between anterior 1/5 and posterior 1/3 of their length. The spermatheca has the
570 corpus narrow throughout, equal in thickness to the collum. The ramus is basally stalked and apically
571 bulbous. The collum exhibits a double-bend, and is recurved.

572 **Description of female**

573 **Habitus** Length 3.46-3.62 mm, width 1.42-1.54 mm, length/width ratio 2.35-2.44, widest at anterior
574 1/6 of elytra. Integument orange-brown to black. Scales with variously interspersed colors ranging
575 from slightly off-white or beige to manila/tan to dark coffee brown, in some specimens appearing
576 semi-translucent (in others opaque). Setae linear to apically explanate, appearing minutely spatulate,
577 sub-recumbent to sub-erect, tan to brown in color.

578 **Mandibles** Covered with white scales, with 2-3 longer setae, and 1-3 shorter setae between these.

579 **Maxillae** Cardo bifurcate at base with an inner angle of ca. 90°, arms roughly equal in length and
580 width, arms of bifurcation equal in length to apically outcurved arm. Stipes sub-rectangular, 1.5× wider
581 than long, roughly equal in width to inner arm of bifurcation of cardo, glabrous. Galeo-lacinial complex
582 nearly extending to apex of maxillary palpomere I; complex mesally membranous, laterally sclerotized,
583 with sharp demarcation of sclerotized region separating palpiger from galeo-lacinial complex; setose in
584 membranous area just adjacent to sclerotized region, setae covering 1/2 of dorsal surface area; dorsally
585 with 5 apicomosal lacinial teeth; ventrally with 3 reduced lacinial teeth. Palpiger with a single lateral seta,
586 otherwise glabrous, anterior 1/2 membranous, posteriorly sclerotized.

587 **Maxillary palps** I apically oblique, apical end forming a 45° angle with base, with 2 apical setae; II
588 sub-cylindrical, with 1 apical seta.

589 **Labium** Prementum roughly pentagonal; apical margins arcuate, medially angulate; lateral margins
590 feebly incurved; basal margin arcuate. Labial palps 3-segmented, I with apical 1/2 projecting beyond
591 margin of prementum, reaching apex of ligula; III slightly longer than II.

592 **Rostrum** Length 0.49-0.50 mm, anterior portion 2.25-2.5× broader than long, rostrum/pronotum length
593 ratio 0.58-0.62, rostrum length/width ratio 1.26-1.32. Separation of rostrum from head generally obscure.
594 Dorsal outline of rostrum nearly square, anterior half of dorsal surface feebly impressed, posterior half
595 coarsely but shallowly punctate to rugose. Rostrum in lateral view nearly square; apical margin strongly
596 bisinuate and emarginate, appearing medially notched, with 2 large vibrissae. Nasal plate lacking distinct
597 impressions, having instead a poorly defined anteromesal convexity, integument completely and evenly
598 covered with white scales. Margins of mandibular incision directed ca. 25-30° outward dorsally in frontal
599 view. Ventrolateral sulci weakly defined as a broad concavity dorsad of insertion point of mandibles,
600 running parallel to scrobe, becoming flatter posteriorly and disappearing ventrally. Dorsal surface of
601 rostrum with median fovea short and linear, or punctate. Rostrum ventrally with sub-parallel sulci
602 beginning at corners of oral cavity and continuing halfway to back of head.

603 **Antennae** Minute tooth formed by overhanging dorsal margin of scrobe anterior to margin of eye by
604 1/3 of length of eye. Scape extending to posterior margin of eye. Terminal funicular antennomere lacking
605 appressed scales, having instead a covering of apically-directed pubescence with interspersed sub-erect
606 setae. Club nearly 3× as long as wide.

607 **Head** Eyes globular and somewhat elongate, strongly impressed, slanted ca. 45° antero-ventrally; eyes
608 separated in dorsal view by 4× their anterior-posterior length, set off from anterior prothoracic margin by
609 1/4 of their anterior-posterior length. Head between eyes punctate and protuberant.

610 **Pronotum** Length/width ratio 0.88-0.89; widest near anterior 2/5; somewhat globular. Anterior margin
611 arcuate, but feebly incurved mesally, lateral margins evenly curved and widening into a bulge just anteriad
612 of midpoint of pronotum, posterior margin straight, with a slight mesal incurvature. Pronotum in lateral
613 view with transverse ventrolateral sulci strongly excavated and distinctly sculptured; with short, recumbent
614 to sub-erect setae that barely attain or reach just beyond anterior margin; these setae becoming shorter
615 and more erect laterally, reaching a maximum length nearly equal to length of eye; dorsally, these setae

616 become uniquely apically explanate, with a longitudinal, medial, ridge-like portion that tapers to either
617 side apicolaterally. Anterolateral margin with a single ocular vibrissa present, emerging near ventral
618 margin of eye; vibrissa achieving a maximum length of 2/5 of anterior-posterior length of eye.

619 **Scutellum** Not exposed.

620 **Pleurites** Metepisternum nearly hidden by elytron except for triangular extension.

621 **Thoracic sterna** Mesocoxal cavities separated by 1/3× width of mesocoxal cavity. Metasternum with
622 transverse sulcus not apparent; metacoxal cavities widely separated by ca. 3× their width.

623 **Legs** Profemur/pronotum length ratio 0.90-0.96; profemur with distal 1/5 produced ventrally as a
624 sub-rectangular projection covering tibial joint; condyle of tibial articulation occupying 4/5 of distal
625 surface and 1/5 length of femur. Protibia/profemur length ratio 0.86-0.91; protibial apex with ventral setal
626 comb recessed in a subtly incurved groove; mucro present as an acute, medially-projected tooth, which is
627 approximately equal in length to surrounding setae. Protarsus with tarsomere III 2× as long as II; wider
628 than long. Metatibial apex with weakly projecting, poorly defined, narrow convexity laterally flanged by
629 5 short, spiniform setae.

630 **Elytra** Length/width ratio 3.03-3.21; widest at anterior 1/6; anterior margins jointly 1.5-2× wider
631 than posterior margin of pronotum; lateral margins nearly straight and sub-parallel after anterior 1/5,
632 converging in posterior 1/3. Posterior declivity angled at 70-75° to main body axis. Elytra with 10
633 complete striae; striae broadly sculpted; punctures broad and faint beneath appressed scales, separated by
634 4-5× their diameter; intervals elevated.

635 **Abdominal sterna** Ventrite III anteromesally incurved around a fovea located mesally on anterior
636 margin, posterior margin elevated and set off from IV along lateral 3/8s of its length. Sternum VII mesally
637 2/3× as long as wide; setae slightly lengthening, and becoming medially directed in posterior 1/3; anterior
638 margin weakly curved; posterior margin distinctly incurved mesally, appearing broadly notched; surface
639 of sternite concave, appearing broadly foveate, immediately anteriad of marginal incurvature.

640 **Tergum** Tergum VII mesally incurved. Pygidium sub-cylindrical; medial 1/3 of anterior 2/3 of pygidium
641 less sclerotized, with a patch of very short, fine setae.

642 **Sternum VIII** Anterior laminar edges each incurved forming a 130° angle with lateral margin; slightly
643 less sclerotized medially between arms; posterior margin medially incurved.

644 **Ovipositor** Coxites as long as broad; styli with 3 setae near the base.

645 **Spermatheca** ?-shaped; collum short, apically with a large, angulate, hood-shaped projection angled
646 at 45° to corpus, sub-equal in length to ramus and contiously aligned with curvature of bulb of ramus;
647 collum sub-contiguous with, and angled at ca. 60° to ramus; ramus basally elongate and constricted,
648 forming a stalk, 1/3× length of collum, bulbous apically, 3× thicker than stalk; corpus not swollen, of
649 equal thickness to collum and cornu; cornu elongate, apically, gradually narrowed, strongly recurved in
650 basal 1/3, straight along mesal 1/3, and curved near apical 1/3 such that apex is parallel to collum and
651 corpus.

652 **Description of male**

653 Not available or known.

654 **Etymology**

655 Named in reference to the short, apically explanate setae interspersed throughout the dorsum, which give
656 this species a distinctly “knobbed” appearance; *tylotos* – knobby; Greek adjective (Brown 1956).

657 **Material examined**

658 **Holotype** ♀ “H. O. Canyon,; Davis Mts., Texas; Jeff Davis County; VII-20-1968, 6200’; J. E. Hafernrik”
659 (**TAMU**).

660 **Paratypes** “24 mi. wsw. Ft. Davis; Jeff Davis Co., Texas; August 17, 1969; Board & Hafernrik” (**TAMU**:
661 1 ♀); “USA Texas Jeff Davis Co.; 4.1 mi. S. Fort Davis; sweeping grasses-weeds; 4750’ . 19.VII.82; R.S.
662 Anderson” (**CMNC**: 1 ♀)

663 ***Distribution***

664 This species has been found in three localities near the Davis Mountains in Jeff Davis County and in nearby
665 Presidio County, Texas (USA). Habitat models (Figs. 36) predict that this represents the northeastern
666 extent of its range, indicating a strong likelihood that it is present in other parts of the northern Chihuahuan
667 desert, especially in the state of Chihuahua (México).

668 ***Natural history***

669 No host plant associations have been documented. It is unknown whether this species is parthenogenetic.

670 **CHECKLIST OF SPECIES**

671 RCC-5 articulations are provided in **bold font**. See Jansen & Franz (2015) for alignments of *Minyomerus*
672 concepts published from 1831 to 2015.

Minyomerus Horn, 1876: 17 sec. Jansen & Franz (2018)

== (INT) AND > (**OST**) *Minyomerus* Horn, 1876 sec. Jansen & Franz (2015)

> AND = *Elissa* Casey, 1888: 271 sec. Casey (1888)

(synonymized by Kissinger, 1964: 30)

> AND = *Pseudelissa* Casey, 1888: 273 sec. Casey (1888)

(synonymized by Pierce, 1909: 359)

> AND = *Piscatopus* Sleeper, 1960: 84 sec. Sleeper (1960)

(synonymized by Jansen & Franz, 2015: 12)

microps (Say, 1831: 9) sec. Jansen & Franz (2015) [redescribed, p. 45]

== (INT) AND > (**OST**) AND = *Minyomerus innocuus* Horn, 1876: 18 sec. Horn (1876)

[former type of *Minyomerus*, designated by Pierce, 1913: 400]

(synonymized by Jansen & Franz, 2015: 45)

== (INT) AND > (**OST**) AND = *Thylacites microps* Say, 1831: 9 sec. Say (1831)

(transferred to *Minyomerus* on the authority of Buchanan *in litt.*

by Blackwelder and Blackwelder, 1948: 46)

== (INT) AND > (**OST**) AND = *Thylacites microsus* Boheman, 1833: 523 sec. Boheman (1833)

(synonymized by LeConte, 1859: 286)

aeriballux Jansen & Franz, 2015: 52 sec. Jansen & Franz (2015)

ampullaceus sp. nov. sec. Jansen & Franz (2018)

bulbifrons Jansen & Franz, 2015: 81 sec. Jansen & Franz (2015)

caseyi (Sharp, 1891: 151) sec. Jansen & Franz (2015) [redescribed, p. 66]

== AND = *Pseudelissa caseyi* Sharp, 1891: 151 sec. Sharp (1891)

(generic name synonymized by Pierce, 1909: 359)

conicollis Green, 1920: 194 sec. Jansen & Franz (2015) [redescribed, p. 33]

constrictus (Casey, 1888: 272) sec. Jansen & Franz (2015) [redescribed, p. 22]

== AND = *Elissa constricta* Casey, 1888: 272 sec. Casey (1888)

(generic name synonymized by Kissinger, 1964: 30)

cracens Jansen & Franz, 2015: 61 sec. Jansen & Franz (2015)

franko sp. nov. sec. Jansen & Franz (2018)

gravivultus Jansen & Franz, 2015: 92 sec. Jansen & Franz (2015)

griseus (Sleeper, 1960: 84) sec. Jansen & Franz (2015) [redescribed, p. 96]

== AND = *Piscatopus griseus* Sleeper, 1960: 84 sec. Sleeper (1960)

(generic name synonymized by Jansen & Franz, 2015: 96)

imberbus Jansen & Franz, 2015: 18 sec. Jansen & Franz (2015)

languidus Horn, 1876: 18 sec. Jansen & Franz (2015) [redescribed, p. 40]

== (INT) AND > (**OST**) *Minyomerus languidus* Horn, 1876: 18 sec. Horn (1876)

== AND = *Pseudelissa cinerea* Casey, 1888: 274 sec. Casey (1888)

(synonymized by Pierce, 1909: 359)

laticeps (Casey, 1888: 272) sec. Jansen & Franz (2015) [redescribed, p. 27]

== AND = *Elissa laticeps* Casey, 1888: 272 sec. Casey (1888)

(generic name synonymized by Kissinger, 1964: 30)

politus Jansen & Franz, 2015: 86 sec. Jansen & Franz (2015)

puticulatus Jansen & Franz, 2015: 75 sec. Jansen & Franz (2015)

reburrus Jansen & Franz, 2015: 57 sec. Jansen & Franz (2015)

rutellirostris Jansen & Franz, 2015: 103 sec. Jansen & Franz (2015)

sculptilis sp. nov. sec. Jansen & Franz (2018)

trisetosus Jansen & Franz, 2015: 71 sec. Jansen & Franz (2015)

tylotos sp. nov. sec. Jansen & Franz (2018)

673 **SPECIES IDENTIFICATION KEY**

- 1 Procoxae apparently separate, with intercoxal processes touching or very nearly so 2
- Procoxae apparently contiguous, with intercoxal processes short and not touching 3
- 2 (1) Rostrum approximately square and as wide as head in dorsal view; ramus of spermatheca basally narrow, forming a stalk that tapers into an apical bulb.....
..... *Minyomerus rutellirostris* [JF2015]
- Rostrum approximately trapezoidal and narrower than the head in dorsal view; ramus of spermatheca cylindrical, somewhat bulbous, and basally constricted ..
..... *Minyomerus griseus* [JF2015]
- 3 (1) Anterior margin of pronotum bearing a full, well-developed tuft of 10 or more ocular vibrissae; anterolateral margins of prementum explanate, angular, and posteriorly declivous, with a distinctly hexagonal appearance..... 4
- Ocular vibrissae reduced in number or length; anterior margins of prementum not explanate and declivous, typically with a pentagonal appearance 5
- 4 (3) Head very wide and only somewhat swollen between eyes; rostrum ca. 4× wider than long in dorsal view; pronotum in dorsal view cylindrical; elytral setae short, brown, and sub-recumbent; ramus of spermatheca stalked and with apical bulb abruptly constricted, not tapering at point of connection to stalk *Minyomerus laticeps* [JF2015]
- Head and rostrum typical (rostrum 2-3× wider than long in dorsal view); pronotum in dorsal view somewhat globular, with a strong anterior constriction; elytral setae short and setiform, especially near disk; spermatheca without basal stalk ..
..... *Minyomerus constrictus* [JF2015]
- 5 (3) Metatibial apex strongly convex, with setae similar in length to those of remainder of leg, somewhat lighter in color and translucent, and slightly lamelliform; head somewhat conical in form, rounded between the eyes; elytral setae copious, not in uniform rows on intervals, instead appearing in offset rows, especially near elytral suture and declivity 6
- Metatibial apex oblique or weakly convex, with setae short and conical in appearance; head roughly quadrate; elytral setae in relatively uniform rows on elytra, not strongly offset.... 7
- 6 (5) Elytral striae deeply and distinctly punctate, appearing pin-striped; elytra without obvious humeri, gradually widening posteriorly; ramus of spermatheca elongate, annulate, and sub-apically situated on corpus..... *Minyomerus aeriballux* [JF2015]
- Elytral striae punctate, with punctures somewhat obscured by appressed scales; elytra somewhat pyriform, with weak, but obviously present humeri; ramus of spermatheca elongate, somewhat swollen, and sub-apically situated on corpus ..
..... *Minyomerus reburrus* [JF2015]
- 7 (5) Elytra very strongly convex in lateral view; anterior margin of pronotum wider than posterior margin; spermatheca comma-shaped, with ramus reduced, apically flattened and sub-contiguous with the collum; aedeagal pedon membranous ventrally, and not fully sclerotized ..
..... *Minyomerus conicollis* [JF2015]
- Elytra only somewhat convex to nearly flat in lateral view; anterior margin of pronotum similar in length to posterior margin; spermatheca variable; aedeagal pedon fully sclerotized ..
..... 8
- 8 (7) Body shape distinctly flask-like, with strongly constricted, sub-cylindrical pronotum and greatly protuberant elytra; in dorsal view, elytra nearly 2× width of pronotum at maximum width and nearly 3/4× as wide as long; in lateral view, anterior and posterior declivities of elytra abrupt and nearly vertical, with anterior elytral margin projecting strongly and characteristically dorsad of articulation with posterior pronotal margin; corpus of spermatheca with highly elongate projection aligned with midline of the ramus, which is basally tapered and angled at nearly 45° to corpus .. *Minyomerus ampullaceus* [JF2018], sp. n.

- Body shape usually narrow; elytra typically not more than $1.5 \times$ width of pronotum and typically not more than $2/3 \times$ as wide as long in dorsal view; elytral declivities in lateral view variable, but anterior margin never abruptly and strongly projected dorsad of posterior pronotal margin; spermatheca variable, but never with elongate projection aligned with midline of ramus 9
- 9 (8) Setae of elytral disc a mix of shorter, brown setae and longer, more erect, white setae 10
- Setae of elytral disc uniform 12
- 10 (9) Anterior margin of pronotum bearing strikingly long setae, which project laterally up to 80° from longitudinal body axis and at least equal to diameter of eye; spermatheca with short, somewhat bulbous corpus, ramus sub-equal in size and perpendicular to corpus, and collum strongly recurved along basal $1/3$ of its length; aedeagal pedon relatively short and wide, and abruptly constricted in apical $1/5$, thereafter tapered to rounded point *Minyomerus franko* [JF2018], sp. n.
- Anterior margin of pronotum bearing setae more strongly directed anteriorly and never as long as diameter of eye; spermatheca variable; aedeagal pedon, where known, narrow and expanded laterally in region of ostium 11
- 11 (10) Setae apically explanate, appearing somewhat spatulate; corpus of spermatheca uniquely elongate, ramus short and cylindrical *Minyomerus caseyi* [JF2015]
- Setae linear; corpus of spermatheca typical, ramus bulbous and basally constricted *Minyomerus trisetosus* [JF2015]
- 12 (9) Anterior margin of pronotum lined with linear setae that extend anteriorly beyond margin by half their length 13
- 675 – Anterior margin of pronotum lacking setae, or with setae that do not extend far beyond margin 14
- 13 (12) Lateral margins of gular cavity strongly rounded, never straight, and slightly longer than posterior margin; frons weakly projected between eyes; appressed scales on elytra without opalescent sheen; nasal plate with or without metallic reflections; lamina of spiculum ventrale sclerotized throughout *Minyomerus languidus* [JF2015]
- Lateral margins of gular cavity nearly straight, and not longer than posterior margin; frons strongly projected between eyes; appressed scales with strong opalescent sheen; nasal plate with metallic reflections; lamina of spiculum ventrale with a membranous region present medially between laminar arm *Minyomerus gravivultus* [JF2015]
- 14 (12) Elytra each $4-5 \times$ as long as broad in dorsal view, strongly punctate; elytra constricted anteriad of humeri, narrower than the pronotum, widening thereafter near the humeri; spermatheca with the corpus somewhat bulbous, and the ramus either flattened somewhat or slightly elongate *Minyomerus cracens* [JF2015]
- Elytra not so elongate, variably punctate; elytra lacking basal constriction; spermatheca variable 15
- 15 (14) Elytral striae with large, obvious punctures 16
- Elytral striae without evident punctures 17
- 16 (15) Frons strongly protuberant; elytra in lateral view convex dorsally; spermatheca with corpus possessing an annulate, rectate projection nearly $1/2 \times$ length of ramus; aedeagal pedon evenly curving towards apex; aedeagal flagellum with spiriform apical sclerite that spirals counterclockwise and of equal length to aedeagal pedon *Minyomerus bulbifrons* [JF2015]

- Frons not so protuberant; elytra in lateral view nearly flat dorsally; spermatheca with corpus possessing an annulate, rectate projection nearly $2/3 \times$ length of the ramus; aedeagal pedon narrow and elongate; aedeagal flagellum with very minute apical sclerite *Minyomerus puticulatus* [JF2015]
- 17 (15) Frons strongly protruding in lateral view by ca. $2 \times$ diameter of eye 18
- Frons not or weakly protruding in lateral view by $1.5 \times$ diameter of eye or less 19
- 18 (17) Nasal plate defined by inversely V-shaped, impressed lines; spermatheca with the ramus elongate and apically swollen, corpus possessing an annulate, rectate projection nearly $1/2 \times$ length of the ramus, and cornu evenly recurved throughout its length; aedeagal flagellum with a spiriform apical sclerite that spirals clockwise and of equal length to pedon *Minyomerus politus* [JF2015]
- Nasal plate lacking distinct impressions; spermatheca with ramus basally tapered with a short stalk, corpus narrow and lacking an annulate rectate bulb, and cornu with an abrupt apical curve; males not known *Minyomerus tylotos* [JF2018], sp. n.
- 19 (17) Ventrolateral sulci weakly defined as a notch ventrad of antennal insertion, or absent entirely; intervals broadly sculpted and raised, and striae not punctate; body generally robust in overall quality; appressed scales uniformly beige and gray, with a distinctly ‘crusty’ appearance; spermatheca with ramus and collum appearing as two subcontiguous, apically invaginated bulbs *Minyomerus microps* [JF2015]
- Ventrolateral sulci deeply and distinctly defined along their entire length; intervals, if raised, only sculpted along lateral faces of elytra, not on disk; body usually not markedly robust; appressed scales either translucent or otherwise typical of genus, not beige and crusted; spermatheca distinctly sinuate, with well defined, protruding ramus 20
- 20 (19) Elytra with very minute setae, only perceptible at high magnification; lateral faces of elytra with intervals not noticeably raised; ramus of spermatheca elongate, cylindrical, and slightly thinner than corpus, cornu strongly recurved in basal half with uniquely sinuate appearance, both corpus and cornu with hood-like projections shorter than ramus; males not known *Minyomerus imberbus* [JF2015]
- Elytra with easily visible, linear setae; lateral faces of elytra with intervals raised; ramus of spermatheca bulbous, basally tapered, and similar in width to corpus, cornu strongly recurved, but short in basal half with uniquely sinuate appearance, both corpus and cornu with hood-like projections longer than ramus; aedeagal pedon narrow and cylindrical, apically tapered *Minyomerus sculptilis* [JF2018], sp. n.

677 PHYLOGENETIC RESULTS

678 A matrix of 52 characters was assembled for the 26 terminal taxa (Tab. 1). These characters are comprised
 679 of all 46 characters included in the revision of *Minyomerus* [JF2015], plus an additional 6 characters
 680 intended to identify putative sister taxa to the newly described species. Parsimony analysis returned a
 681 single, most-parsimonious cladogram (henceforth MPT) with a length (L) of 99 steps, a consistency index
 682 (CI) of 60 and a retention index (RI) of 80 (Farris 1989); see Figs. 30-31. TNT (Tree Analysis Using
 683 New Technology) was used to confirm that the shortest tree had been found (Goloboff et al. 2008). The
 684 most-parsimonious cladogram is shown in Fig. 30, with relative and absolute Bremer support values
 685 (see also **Materials and Methods: Phylogenetic analysis**) mapped along the left side of each branch;
 686 nodes with bootstrap support above 0.95 are marked with a “*” symbol to the right of each node. In a
 687 complementary graph, we show the herein used clade concept labels (Fig. 31).

688 The characters, states, and preferred optimizations are described in this section. Characters relating
 689 to placement of the herein described taxa are discussed in detail in the **Discussion** section, along with
 690 changes in species group composition and tree topology from Jansen & Franz (2015). For all characters
 691 not resolved as unreversed synapomorphies, both the individual consistency (ci) and retention (ri) indices
 692 are provided. Characters are numbered in accordance with descriptive sequence used in the species
 693 accounts. A “–” symbol indicates inapplicable (character, state), whereas a “?” symbol indicates missing
 694 information, e.g., due to the unavailability of male specimens or insufficient specimens on hand to permit
 695 full dissections. Characters 9, 27, 39, 45 - 47, 49, and 51 were mapped onto the preferred phylogeny
 696 using ACCTRAN optimization (see Agnarsson & Miller 2008), and the remaining characters had an
 697 unambiguous optimization.

Table 1. Taxon/character matrix used for for cladistic analysis. Includes all species of *Minyomerus* [JF2015], newly designated species, and select outgroup taxa. All multi-state characters coded as additive, except for character 33. The symbol “–” denotes inapplicable character states, whereas “?” denotes missing information (see also text).

Taxon \ Character	0 5	1 0	1 5	2 0	2 5	3 0	3 5	4 0	4 5	5 0
<i>Sitona californicus</i> [non-focal]	00-00	?????	00000	00000	00000	00000	00---	-0---	--???	????? ??
<i>Pandeleteius cinereus</i> [non-focal]	11000	?????	01000	00001	01000	00100	00000	000-0	002???	????? ??
<i>Pandeleteinus subcancer</i> [non-focal]	11000	?????	01000	00001	01010	00100	00000	000-0	002???	????? ??
<i>Isodrusus debilis</i> [non-focal]	11000	?????	01000	00001	01011	00100	00000	000-0	002???	????? ??
<i>Isodacrys buchanani</i> [non-focal]	11000	?????	01000	00001	01011	00101	00000	000-0	002???	????? ??
<i>Minyomerus constrictus</i> [JF2015]	21100	00010	02110	01002	00011	11211	00000	00000	01010	00
<i>Minyomerus laticeps</i> [JF2015]	21100	00010	02110	01002	00011	11211	00000	00000	01010	00
<i>Minyomerus imberbus</i> [JF2015]	21100	?????	02010	11002	10011	11211	01001	00000	002???	????? ??
<i>Minyomerus sculptilis</i> [JF2018]	21100	?????	02010	11002	10011	11211	01001	00000	00001	00000 10
<i>Minyomerus conicollis</i> [JF2015]	21100	00000	02010	11002	10011	10211	00001	10000	01000	00000 00
<i>Minyomerus languidus</i> [JF2015]	21000	11100	02010	11002	10011	10211	00001	10000	?????	????? ??
<i>Minyomerus microps</i> [JF2015]	21001	11101	02110	11002	10011	10211	00001	10000	10???	????? ??
<i>Minyomerus tylotos</i> [JF2018]	21001	11101	02110	11002	10011	10211	00001	10000	002???	????? ??
<i>Minyomerus cracens</i> [JF2015]	21000	11101	02020	11112	10011	11211	00001	10001	00000	10010 10
<i>Minyomerus ampullaceus</i> [JF2018]	21000	?????	02020	11???	10011	11211	00001	11001	002???	????? ??
<i>Minyomerus aeriballux</i> [JF2015]	22000	11101	12020	11012	10011	20211	00001	11001	10000	00000 01
<i>Minyomerus reburrus</i> [JF2015]	22000	11101	12020	11112	10011	20211	00001	11021	002???	????? ??
<i>Minyomerus franko</i> [JF2018]	21110	10100	02020	11002	10011	11211	00001	10011	10010	00000 01
<i>Minyomerus caseyi</i> [JF2015]	21110	00101	02020	11112	10011	11211	00001	10101	10010	10010 01
<i>Minyomerus trisetosus</i> [JF2015]	21110	00101	02020	11012	10011	10211	00001	10101	10???	????? ??
<i>Minyomerus gravivultus</i> [JF2015]	21100	11101	02120	11002	10011	10211	00111	10000	?2010	00000 11
<i>Minyomerus griseus</i> [JF2015]	21100	10101	02120	01002	10111	11211	00111	10000	00010	01100 10
<i>Minyomerus rutellirostris</i> [JF2015]	21100	10101	02120	11002	10111	11211	00111	10000	00010	01100 10
<i>Minyomerus puticalutus</i> [JF2015]	21000	11101	02020	11012	10011	11211	10101	10010	01011	01000 11
<i>Minyomerus bulbifrons</i> [JF2015]	21000	11101	02021	11112	10011	10211	10101	10000	01110	01001 01
<i>Minyomerus politus</i> [JF2015]	21000	?????	02021	11112	10011	10211	10101	10010	01111	01001 11

- 698 1. Habitus, form of appressed scales: (0) elongate pyriform, not overlapping; (1) sub-circular to
 699 polygonal, variously overlapping non-linearly; (2) sub-circular and only overlapping posteriorly.
 700 Coded as additive due to alignment of character states with the preferred phylogeny. Coding as
 701 non-additive in isolation or in unison with other additive multi-state characters does not affect
 702 polarization of the character/states or alter the phylogeny. State 1 is a synapomorphy for the
 703 tanymecine clade [non-focal], whereas state 2 is a synapomorphy for *Minyomerus* [JF2018].
- 704 2. Habitus, arrangement of elytral setae: (0) variously interspersed; (1) arranged in single-file rows
 705 on elytral intervals; (2) arranged non-uniformly on elytral intervals. Coded as additive due to
 706 alignment of character states with the preferred phylogeny. Coding as non-additive in isolation or in
 707 unison with other additive multi-state characters does not affect polarization of the character/states
 708 or alter the phylogeny. State 1 is a synapomorphy for the tanymecine clade [non-focal], whereas
 709 state 2 is a synapomorphy the *M. aeriballux*–*M. reburrus* clade [JF2015].
- 710 3. Habitus, lateral elytral setae and ventral setae differentiated from setae of elytral disc: (0) absent;
 711 (1) present. Homoplasy for *Minyomerus* [JF2018], with a reversal (state 0) in the *M. aeriballux*–*M.*
 712 *languidus* clade [JF2015], subsequent convergent gain (state 1) in the *M. bulbifrons*–*M. caseyi* clade
 713 [JF2018], and convergent reversal (state 0) in the *M. bulbifrons*–*M. puticalutus* clade [JF2015] (ci =
 714 25; ri = 70).
- 715 4. Habitus, rows of elytral setae with larger white setae randomly interspersed among smaller brown
 716 setae: (0) absent; (1) present. Synapomorphy for the *M. caseyi*–*M. franko* clade [JF2018]. Changed
 717 from Jansen & Franz (2015), where *M. rutellirostris* [JF2015] was previously coded as having this
 718 character; however, the white elytral setae of this species are not randomly interspersed, but follow
 719 a distinct, and uniquely derived, pattern where every other interval contains a row of such setae.
- 720 5. Habitus, elytra and pronotum generally large, protuberant, and sculpted in appearance along dorsal
 721 and lateral faces: (0) absent; (1) present. Synapomorphy for the *M. microps*–*M. tylotos* clade
 722 [JF2018].

6. Prementum, anterior margin forming a distinct face that continues to lateral margins: (0) absent; (1) present. Synapomorphy for the *M. aeriballux*–*M. languidus* clade [JF2015], with a single reversal in the *M. caseyi*–*M. trisetosus* clade [JF2015] (ci = 50; ri = 75).
7. Prementum, strongly ligulate and with margins nearly straight, appearing pentagonal: (0) absent; (1) present. Synapomorphy for the *M. aeriballux*–*M. languidus* clade [JF2015], with independent reversals in the *M. caseyi*–*M. franko* clade [JF2018] and *M. griseus*–*M. rutellirostris* clade [JF2015], respectively (ci = 33; ri = 71).
8. Prementum, anterolateral margins simple, unexpanded: (0) absent; (1) present. Synapomorphy for the *M. aeriballux*–*M. languidus* clade [JF2015].
9. Prementum, anterolateral margins explanate, angular, and posteriorly declivous, with a distinctly hexagonal appearance: (0) absent; (1) present. ACCTRAN optimization preferred (see Agnarsson & Miller 2008), therefore inferred as a synapomorphy for the *M. constrictus*–*M. laticeps* clade [JF2015].
10. Prementum, exposure of palpomere I: (0) exposed, visible beyond ligula and anterior margin of prementum in ventral view; (1) hidden, fully covered or only minutely exposed beyond ligula and anterior margin of prementum in ventral view. Synapomorphy for the *M. aeriballux*–*M. microps* clade [JF2015], with a single reversal in *M. franko* [JF2018] (ci = 50; ri = 75).
11. Rostrum, form in dorsal view: (0) approximately quadrate; (1) somewhat conical, medially convex. Synapomorphy for the *M. aeriballux*–*M. reburrus* clade [JF2015].
12. Rostrum, form of nasal plate and demarcation of epistoma: (0) with three parallel, longitudinal carinae, and surface planar between these; (1) with a sharp, narrow, chevron-shaped carina demarcating epistoma; (2) with a broad, scale-covered, chevron-shaped carina demarcating epistoma. Coded as additive due to alignment of character states with preferred phylogeny. Coding as non-additive in isolation or in unison with other additive multi-state characters does not affect polarization of the character/states or alter the phylogeny. State 1 is a synapomorphy for the tanymecine clade [non-focal], whereas state 2 is a synapomorphy for *Minyomerus* [JF2018].
13. Rostrum, sulcus posteriad of nasal plate weakly impressed: (0) absent; (1) present. Convergently present in the *M. constrictus*–*M. laticeps* clade [JF2015], the *M. microps*–*M. tylotos* clade [JF2018], and the *M. gravivultus*–*M. griseus* clade [JF2015] (ci = 33; ri = 60).
14. Rostrum, form of sulcus posteriad of nasal plate: (0) absent; (1) sulcus present, broad, and weakly punctate; (2) sulcus present, more strongly punctate. Coded as additive due to alignment of character states with preferred phylogeny. Coding as non-additive in isolation or in unison with other additive multi-state characters does not affect polarization of the character/states or alter the phylogeny. Synapomorphy for *Minyomerus* [JF2018] (state 1) and the *M. aeriballux*–*M. cracens* clade [JF2015] (state 2), respectively.
15. Head, frons very strongly projected beyond anterior margin of eye, by $2 \times$ anterior-posterior length of eye: (0) absent; (1) present. Synapomorphy for the *M. bulbifrons*–*M. politus* clade [JF2015].
16. Head, frons with posterior transverse constriction: (0) absent; (1) present. Synapomorphy for the *M. aeriballux*–*M. languidus* clade [JF2015], with a single reversal in *M. griseus* [JF2015] (ci = 50, ri = 85).
17. Antenna, length of scrobe relative to funicle and club: (0) scrobe shorter than funicle and club combined; (1) scrobe subequal in length to funicle and club combined. Synapomorphy for *Minyomerus* [JF2018].
18. Antenna, terminal funicular segment entirely without thin, nearly setiform scales: (0) absent; (1) present. Convergently present in *M. cracens* [JF2015], *M. reburrus* [JF2015], *M. caseyi* [JF2015], and the *M. bulbifrons*–*M. politus* clade [JF2015] (ci = 25; ri = 25).

- 769 19. Antenna, terminal funicular segment at least partially clothed with broad scales: (0) absent; (1)
 770 present. Synapomorphy for the *M. aeriballux*–*M. cracens* clade [JF2018] with independent reversals
 771 in *M. franko* [JF2018] and the *M. gravivultus*–*M. griseus* clade [JF2015] (ci = 33; ri = 71).
- 772 20. Head, angle of base in relation to prothorax: (0) directed anteriorly, in line with main body axis; (1)
 773 directed strongly ventrally; (2) directed slightly ventrally. Coded as additive due to alignment of
 774 character states with preferred phylogeny. Coding as non-additive in isolation or in unison with
 775 other additive multi-state characters does not affect polarization of the character/states or alter the
 776 phylogeny. State 1 is a synapomorphy for the tanymecine clade [non-focal], whereas state 2 is a
 777 synapomorphy for *Minyomerus* [JF2018].
- 778 21. Pronotum, condition of post-ocular vibrissae: (0) present in a well-developed tuft of 10 or more
 779 setae; (1) present in a reduced tuft of 3-7 setae. Synapomorphy for the *M. aeriballux*–*M. imberbus*
 780 clade [JF2018].
- 781 22. Prosternum, intercoxal process complete, undivided: (0) absent; (1) present. Synapomorphy for the
 782 tanymecine clade [non-focal], with a single reversal for *Minyomerus* [JF2018] (ci = 50; ri = 66).
- 783 23. Prosternum, intercoxal process divided at midpoint between coxae, but both anterior and posterior
 784 processes extending completely between procoxae and contiguous with each other: (0) absent; (1)
 785 present. Synapomorphy for the *M. griseus*–*M. rutellirostris* clade [JF2015].
- 786 24. Legs, fore femora not swollen in comparison to other legs: (0) absent; (1) present. Synapomorphy
 787 for the *M. aeriballux*–*P. subcancer* clade [non-focal].
- 788 25. Legs, sculpture of ventral surface of protibiae: (0) evenly convex throughout; (1) with a longitudinal
 789 groove or concavity. Synapomorphy for the *M. aeriballux*–*I. debilis* clade [non-focal].
- 790 26. Legs, setation of metatibial apex: (0) bristles at least as long as surrounding setae and setiform; (1)
 791 bristles shorter than surrounding setae and conical; (2) bristles sub-equal in length to surrounding
 792 setae and somewhat lamelliform. Coded as additive due to alignment of character states with
 793 preferred phylogeny, and the appearance of being a transformation series. Coding as non-additive
 794 in isolation or in unison with other additive multi-state characters does not affect polarization of the
 795 character/states or alter the phylogeny. Synapomorphy for *Minyomerus* [JF2018] (state 1) and the
 796 *M. aeriballux*–*M. reburrus* clade [JF2015] (state 2), respectively.
- 797 27. Legs, curvature of metatibial apex: (0) convex ; (1) oblique. ACCTRAN optimization preferred
 798 (see Agnarsson & Miller 2008), therefore inferred as a synapomorphy for *Minyomerus* [JF2018]
 799 with a reversal (state 0) in the *M. aeriballux*–*M. conicollis* clade [JF2015], then a convergent gain
 800 (state 1) in the *M. aeriballux*–*M. bulbifrons* clade [JF2018], with independent reversals (state 0) in
 801 the *M. aeriballux*–*M. reburrus* clade [JF2015], *M. gravivultus* [JF2015], *M. trisetosus* [JF2015],
 802 and the *M. bulbifrons*–*M. politus* clade [JF2015] (ci = 14; ri = 40).
- 803 28. Legs, relative length of mesotarsi to mesotibiae: (0) tarsi much shorter than tibiae; (1) tarsi at least
 804 equal in length to tibiae; (2) tarsi slightly shorter than tibiae. Coded as additive due to alignment of
 805 character states with preferred phylogeny. Coding as non-additive in isolation or in unison with
 806 other additive multi-state characters does not affect polarization of the character/states or alter the
 807 phylogeny. State 1 is a synapomorphy for the tanymecine clade [non-focal], whereas state 2 is a
 808 synapomorphy for *Minyomerus* [JF2018].
- 809 29. Legs, tarsi ventrally spinose: (0) absent; (1) present. Synapomorphy for *Minyomerus* [JF2018].
- 810 30. Elytra, humeral angle rounded, not projected: (0) absent; (1) present. Synapomorphy for the *M.*
 811 *aeriballux*–*I. buchanani* clade [non-focal].
- 812 31. Female terminalia, spermatheca with apical cylindrical bulb on corpus: (0) absent; (1) present.
 813 Synapomorphy for the *M. bulbifrons*–*M. puticulatus* clade [JF2015].
- 814 32. Female terminalia, corpus of spermatheca sinuate: (0) absent; (1) present. Synapomorphy for the
 815 *M. imberbus*–*M. sculptilis* clade [JF2018].

- 816 33. Female terminalia, lamina of spiculum ventrale less sclerotized between laminar arms: (0) absent;
 817 (1) present. Coded as inapplicable for *S. californicus* [non-focal], as laminar arms are not apparent.
 818 Synapomorphy for the *M. gravivultus*–*M. griseus* clade [JF2015].
- 819 34. Female terminalia, lamina of spiculum ventrale with laminar arms bifurcating around a membranous
 820 region: (0) absent; (1) present. Coded as inapplicable for *S. californicus* [non-focal], as laminar
 821 arms are not apparent. Synapomorphy for the *M. gravivultus*–*M. griseus* clade [JF2015].
- 822 35. Female terminalia, lamina of spiculum ventrale with style basally divided or obscured, not mesally
 823 intact: (0) absent; (1) present. Coded as inapplicable for *S. californicus* [non-focal], as laminar
 824 arms are not apparent. Synapomorphy for the *M. aeriballux*–*M. imberbus* clade [JF2015].
- 825 36. Female terminalia, lamina of spiculum ventrale with laminar arms clearly bifurcating. (0) absent;
 826 (1) present. Coded as inapplicable for *S. californicus* [non-focal], as laminar arms are not apparent.
 827 Synapomorphy for the *M. aeriballux*–*M. conicollis* clade [JF2015].
- 828 37. Female terminalia, laminar arms narrowly bifurcating basally, thereafter sub-parallel mesally: (0)
 829 absent; (1) present. Synapomorphy for the *M. aeriballux*–*M. ampullaceus* clade [JF2018].
- 830 38. Female terminalia, coxites of ovipositor with a lateral, anteriorly-directed, recurved, alate process:
 831 (0) absent; (1) present. Coded as inapplicable for *S. californicus* [non-focal], as coxites of ovipositor
 832 are not apparent. Synapomorphy for the *M. caseyi*–*M. trisetosus* clade [JF2015].
- 833 39. Female terminalia, relative length of styli to coxites of ovipositor: (0) Similar in size; (1) distinctly
 834 shortened; (2) highly reduced, appearing minute. Coded as non-additive, due to strong differences
 835 in structure of coxites and styli in state 2; inapplicable for outgroup taxa, as styli of ovipositor are
 836 not apparent. ACCTRAN optimization preferred (see Agnarsson & Miller 2008), therefore inferred
 837 as convergent gains in *M. franko* [JF2018] and the *M. bulbifrons*–*M. puticulatus* clade [JF2015]
 838 (state 1), with a single reversal in *M. bulbifrons* [JF2015] (state 0). Autapomorphy for *M. reburrus*
 839 [JF2015] (state 2) (ci = 50, ri = 0).
- 840 40. Female terminalia, condition of medial, anteriorly-directed, sclerotized process of coxites of
 841 ovipositor: (0) fully developed; (1) reduced and inapparent. Coded as inapplicable for *S. californicus*
 842 [non-focal], as coxites of ovipositor are not apparent. Synapomorphy for the *M. aeriballux*–*M.*
 843 *cracens* clade [JF2015], with a single reversal in the *M. gravivultus*–*M. griseus* clade [JF2015] (ci
 844 = 50, ri = 83).
- 845 41. Female terminalia, anterior margin of tergum VII entirely free of sclerotized band: (0) absent;
 846 (1) present. Coded as inapplicable for *S. californicus* [non-focal], as the tergum VII is evenly
 847 sclerotized throughout. Convergently present in *M. aeriballux* [JF2015], *M. microps* [JF2015], and
 848 the *M. caseyi*–*M. trisetosus* clade [JF2018] (ci = 33; ri = 50).
- 849 42. Female terminalia, anterior margin of tergum VII sclerotized fully, appearing as an obviously
 850 complete band: (0) absent; (1) present. Coded as inapplicable for *S. californicus* [non-focal], as the
 851 tergum VII is evenly sclerotized throughout. Convergently present in *M. conicollis* [JF2015] and
 852 the *M. bulbifrons*–*M. puticulatus* clade [JF2015] (ci = 50; ri = 66).
- 853 43. Male terminalia, apical sclerite of aedeagal flagellum elongate-spiriform: (0) absent; (1) present.
 854 Synapomorphy for the *M. bulbifrons*–*M. politus* clade [JF2015].
- 855 44. Male terminalia, style of spiculum gastrale with an anterior ventral flange: (0) absent; (1) present.
 856 Synapomorphy for the *M. bulbifrons*–*M. caseyi* clade [JF2018].
- 857 45. Male terminalia, lamina of spiculum gastrale longer than broad and anteriorly extended along
 858 syle: (0) absent; (1) present. ACCTRAN optimization preferred (see Agnarsson & Miller 2008),
 859 therefore inferred as convergent gains in the *M. imberbus*–*M. sculptilis* clade [JF2018] and the *M.*
 860 *bulbifrons*–*M. puticulatus* clade [JF2015], with a reversal in *M. bulbifrons* [JF2015] (ci = 33; ri =
 861 0).

- 862 46. Male terminalia, sub-triangular sclerites of sternum VIII with a medial process: (0) absent; (1)
 863 present. ACCTRAN optimization preferred (see Agnarsson & Miller 2008), therefore inferred as
 864 convergent gains in *M. cracens* [JF2015] and the *M. caseyi*–*M. trisetosus* clade [JF2015] (ci =
 865 50, ri = 0).
- 866 47. Male terminalia, curvature of posterior margin of tergum VII: (0) evenly arcuate; (1) medially
 867 incurved. ACCTRAN optimization preferred (see Agnarsson & Miller 2008), therefore convergently
 868 present in the *M. constrictus*–*M. laticeps* clade [JF2015] and the *M. bulbifrons*–*M. gravivultus* clade
 869 [JF2015] with a reversal in *M. gravivultus* [JF2015] (ci = 33; ri = 66).
- 870 48. Male terminalia, tergum VII approximately 4× as long as broad: (0) absent; (1) present. Synapo-
 871 mophy for the *M. griseus*–*M. rutellirostris* clade [JF2015].
- 872 49. Male terminalia, aedeagal pedon expanded laterally around ostium: (0) absent; (1) present. ACC-
 873 TRAN optimization preferred (see Agnarsson & Miller 2008), therefore convergently present in the
 874 *M. constrictus*–*M. laticeps* clade [JF2015], *M. cracens* [JF2015], and the *M. caseyi*–*M. trisetosus*
 875 clade [JF2015] (ci = 33; ri = 33).
- 876 50. Male terminalia, aedeagal pedon broad basally, evenly tapering toward apex: (0) absent; (1) present.
 877 Synapomorphy for the *M. bulbifrons*–*M. politus* clade [JF2015].
- 878 51. Male terminalia, aedeagal pedon medially sclerotized along dorsum: (0) absent; (1) present.
 879 ACCTRAN optimization preferred (see Agnarsson & Miller 2008), therefore convergently present
 880 in the *M. imberbus*–*M. sculptilis* clade [JF2015], *M. cracens* [JF2015], and the *M. bulbifrons*–*M.*
 881 *gravivultus* clade [JF2015], with a reversal in *M. bulbifrons* [JF2015] (ci = 25; ri = 50).
- 882 52. Male terminalia, width of connection between apodemes of aedeagal tegmen: (0) wider than base of
 883 apodeme; (1) narrower than base of apodeme. Synapomorphy for the *M. aeriballux*–*M. bulbifrons*
 884 clade [JF2018], with a single reversal in the *M. griseus*–*M. rutellirostris* clade [JF201] (ci = 50; ri
 885 = 83).

RCC–5 ALIGNMENTS

887 Details of our RCC–5 alignment approached are given in free text form in the **Supplemental Information**
 888 **SI1**, which also describes the content of the data input and output files. The latter, in turn, are appended
 889 in .txt, .csv, and .pdf format in the **Supplemental Information SI2 to S4**. All shown alignments are
 890 *intensional* in the sense of Franz & Peet (2009), and thus maximize high-level concept congruence where
 891 indicated, and in spite of non-congruent lower-level concept sampling.

892 The first, classification-based alignment (Fig. 32) is simple and straightforward to interpret (see also
 893 **Supplemental Information SI2**). We obtain high-level congruence among the concepts *Minyomerus*
 894 [JF2018] and *Minyomerus* [JF2015], where 17 species-level concepts are retained from Jansen & Franz
 895 (2015) and four species-level concepts are added in the current revision. The coverage constraint is
 896 relaxed for *Minyomerus* [JF2015], thus allowing the four new species-level concepts to be subsumed
 897 under this parent. This is based on our assertion that they fall under the generic character circumscription
 898 of Jansen & Franz (2015).

899 The following two Figs. 33–34 show fully bifurcated, multi-phylogeny alignments of the same reasoner
 900 toolkit input, but resolved as whole concepts versus split concepts, respectively. In Fig. 33 (**Supplemental**
 901 **Information SI3**), we observe that the phylogenetic placements of *two* of the four new species-level
 902 concepts cause significant non-congruence in the alignment, resulting in seven overlapping RCC–5
 903 articulations. *Minyomerus franko* [JF2018] is subsumed under the *M. caseyi*–*M. franko* clade [JF2018],
 904 which is intensionally congruent with the *M. caseyi*–*M. trisetosus* clade [JF2015]. In other words, this
 905 placement is not the source of non-congruence in the alignment. Similarly, the placement of *M. tylotos*
 906 [JF2018] into the new *M. microps*–*M. tylotos* clade [JF2018] is not conflicting in an intensional sense. At
 907 the next, more inclusive level, this addition “resolves” into the congruent *M. aeriballux*–*M. microps* clade
 908 [JF2018]/[JF2015].

909 In contrast, the placement of *M. ampullaceus* [JF2018] “inside” of *M. cracens* [JF2015] in the current
 910 phylogeny, generates five overlapping articulations among as many (five) non-congruent concept regions
 911 positioned 1–2 levels above these species-level concepts. The conflict is resolved in the next, more

inclusive and congruent region of the *M. aeriballux*–*M. cracens* clade [JF2018] == *M. aeriballux*–*M. bulbifrons* clade [JF2015]

The placements of the previously circumscribed *M. imberbus* [JF2015] and the new species-level concept *M. sculptilis* [JF2018] - in relation to the congruent clade *M. constrictus*–*M. laticeps* [JF2018]/[JF2015] - cause two additional instances of overlap (Fig. 33). In the current phylogeny, *M. imberbus* [JF2015] is sister to *M. sculptilis* [JF2018], and placed “inside” of the *M. constrictus*–*M. laticeps* clade [JF2018]/[JF2015]. However, in the preceding phylogeny sec. Jansen & Franz (2015), *M. imberbus* [JF2015] is non-congruently included in the *M. constrictus*–*M. imberbus* clade [JF2015]. This conflict is only resolved at the level of *Minyomerus* [JF2018]/[JF2015].

Figure 34 (**Supplemental Information SI4**) shows that the inclusion of the four new species-level concepts in the *Minyomerus* [JF2018] phylogeny generates five split-concept regions for which there are no adequate labels in either input phylogeny. These labels correspond to the overlapping articulations mentioned above; in particular the non-congruent assignments of *M. ampullaceus* [JF2018], *M. cracens* [JF2018], and *M. sculptilis* [JF2018]. The phylogenetic character evidence for these placements and relationships are discussed in the following sections.

DISCUSSION

Relationships to the previous revision

The differences of the current phylogeny (Figs. 30-31) in relation to that of Jansen & Franz (2015) are in large part due to the unique character combinations present in the newly added species (Rieppel 2007, Franz 2014). Nonetheless, three main clades are resolved with strong support, and further corroborate the topology of Jansen & Franz (2015), as follows:

1. *Minyomerus* [JF2018] is strongly supported by the same eight synapomorphies identified in Jansen & Franz (2015). These are reiterated in the Introduction (Bremer support value [henceforth: bsv] = 10, relative fit difference [henceforth: rfd] = 95; Bootstrap [henceforth: boot] = 100).
2. *Minyomerus griseus* [JF2015] forms a well-supported clade with *M. rutellirostris* [JF2015] (bsv = 4, rfd = 77, boot = 96). These taxa jointly share the same two synapomorphies (chars. 23:1 and 48:1) provided in Jansen & Franz (2015): (1) the intercoxal process is divided at the midpoint between the coxae, but has both the anterior and posterior processes extending completely between the procoxae and contiguous with each other; and (2) the male tergum VII is nearly 4× as long as broad, respectively. In addition, the *M. gravivultus*–*M. griseus* [JF2015] clade (bsv = 3, rfd = 60), as resolved in the current cladogram, is congruent with that of Jansen & Franz (2015).
3. *Minyomerus* [JF2018] is nested within a well-supported clade of Tanymercini [non-focal] (boot = 100). However, further work is needed to assess the phylogenetic relationships between all genera presently assigned to the Tanymercini [non-focal] (Alonso-Zarazaga & Lyal 1999).

Intrageneric relationships

Within *Minyomerus* [JF2018], beginning at the earliest-bifurcating node and proceeding towards the leaves, the first major incongruence with *Minyomerus* [JF2015] is the placement of *M. imberbus* [JF2015]. This species was sister to the *M. constrictus*–*M. laticeps* [JF2015] clade, which in turn was sister to the *M. aeriballux*–*M. conicollis* clade [JF2015]. The present analysis places *M. imberbus* [JF2015] in a clade with *M. sculptilis* [JF2018] (see **Placement of newly described species**). The *M. aeriballux*–*M. imberbus* clade [JF2018] (bsf = 2, rfd = 50) is supported by three synapomorphies: (1) presence of a transverse constriction across the posterior of the frons (char. 16: 1); (2) presence of a reduced tuft of post-ocular vibrissae (char. 21: 1); and (3) a mesally obscure lamina of the spiculum ventrale in the female (char. 35: 1).

We resolve *M. cracens* [JF2015] as sister to the *M. aeriballux*–*M. bulbifrons* [JF2018] clade, inclusively supported by three synapomorphies: (1) presence of a strongly punctate sulcus posteriad of the nasal plate (char. 14: 2); (2) presence of broad scales on the terminal funicular segment of the antennae (char. 19: 1); and (3) absence of a medial, anteriorly-directed, sclerotized process on the coxites of the ovipositor (char. 40: 1).

The *M. aeriballux*–*M. bulbifrons* [JF2018] clade is weakly supported by a single synapomorphy: the width of the connection between the apodemes of the aedeagal tegmen is narrower than the base of the

963 apodeme (char. 52: 1). Within this clade, the position of the *M. bulbifrons*–*M. caseyi* clade [JF2018] clade
964 as separate from, and sister to, the *M. aeriballux*–*M. ampullaceus* clade [JF2018], is supported by one
965 synapomorphy and one homoplasious character, namely: (1) presence of an anterior ventral flange on the
966 style of the spiculum gastrale (char. 44: 1 – synapomorphic), and (2) differentiation of the setae on the
967 lateral portion of the elytra and on the venter from the setae on the elytral disc (char. 3: 1 – homoplasious).

968 **Placement of newly described species**

969 Clades within *Minyomerus* [JF2018] not addressed in the preceding section are identical in topology and
970 composition to those of *Minyomerus* [JF2015], except for the addition of newly described species. Here
971 we assess the phylogenetic placements of these species. We also discuss similarities in the biogeographic
972 range of each species, in relation to the putative sister taxa, based on the results of species distribution
973 modeling (see Figs. 35–38).

974 ***Minyomerus sculptilis* [JF2018]**

975 *Myriomerus sculptilis* [JF2018] is inferred as sister to *M. imberbus* [JF2015]. The *M. imberbus*–*M.*
976 *sculptilis* clade [JF2018] (bsv = 3, rfd = 72) is supported by a single synapomorphy and two homoplasious
977 characters: (1) corpus of spermatheca sinuate (char. 32: 1 – synapomorphic); (2) lamina of spiculum
978 gastrale in male longer than broad and anteriorly extended along style (char. 45: 1 – homoplasious); and
979 (3) aedeagal pedon medially sclerotized along dorsum (char. 51: 1 – homoplasious). In addition to these
980 characters, *M. imberbus* [JF2015] and *M. sculptilis* [JF2018] share a general external gestalt, which makes
981 separating these two species difficult, especially in damaged or worn specimens.

982 Whereas *M. sculptilis* [JF2018] is associated with big sagebrush (*Artemisia tridentata* [non-focal]),
983 tumbleweed (*Salsola tragus* [non-focal]), and tall tumblemustard (*Sisymbrium altissimum* [non-focal]);
984 its sister taxon *M. imberbus* [JF2015] is associated with budsage (*Artemisia spinescens* [non-focal]).
985 The divergence of these two species may have been driven in part by differences in host-plant use.
986 However, this is less likely considering the generalist feeding habits of *Minyomerus* [JF2018] congeners.
987 Conversely, their divergence may have resulted from a vicariance event, based on their present-day
988 biogeographic distributions, which are separated by the eastern extension of the Columbia Plateau.
989 *Minyomerus sculptilis* [JF2018] appears to be endemic to the Snake River Plain to the north, whereas *M.*
990 *imberbus* [JF2015] has been found in the Great Basin Desert to the south.

991 ***Minyomerus tylotos* [JF2018]**

992 *Minyomerus tylotos* [JF2018] is sister to *M. microps* [JF2015]. The *M. microps*–*M. tylotos* clade [JF2018]
993 (bsv = 3, rfd = 73) is supported by a single synapomorphy and a single homoplasious character: (1) elytra
994 and pronotum generally large, protuberant, and sculpted in appearance along dorsal and lateral faces (char.
995 5: 1 – synapomorphic); and (2) sulcus posteriad of nasal plate broad and weakly punctate (char. 13: 1 –
996 homoplasious). In addition to these characters, the two species share a similar gestalt and uniform setation.

997 *Minyomerus tylotos* [JF2018] appears to be endemic to northern Chihuahuan Desert, whereas *M.*
998 *microps* [JF2015] is widely distributed to the north throughout the Great Plains and along the Missouri
999 River. We consider it likely that *M. microps* [JF2015] represents a northern radiation of the common
1000 ancestor of this clade. Conversely, *M. tylotos* [JF2018] may represent the ancestral distribution to the
1001 south, based on the hypothesized origin of *Minyomerus* [JF2018] in the Chihuahuan Desert; see Jansen &
1002 Franz (2015) and Wilson & Pitts 2010.

1003 ***Minyomerus ampullaceus* [JF2018]**

1004 *Minyomerus ampullaceus* [JF2018] is sister to the *M. aeriballux*–*M. reburrus* clade [JF2015]. The *M.*
1005 *aeriballux*–*M. ampullaceus* clade [JF2018] (bsv = 1, rfd = 50) is supported by a single synapomorphy:
1006 lamina of spiculum ventrale with laminar arms basally bifurcating and sub-parallel mesally thereafter
1007 (char. 37: 1). The placement of this species is tentative and based on the characteristics of a single, worn
1008 specimen.

1009 Nonetheless, the biogeographic distributions of the species in the *M. aeriballux*–*M. ampullaceus*
1010 clade [JF2018] exhibit overlap. *Minyomerus ampullaceus* [JF2018] is documented from Carlsbad, New
1011 Mexico, in the western parts of the distributions of *M. aeriballux* [JF2015] and *M. reburrus* [JF2015].
1012 The divergence of the latter two species is thought to be a result of their habitat and host plant preference,
1013 given their overlapping ranges. *Minyomerus aeriballux* [JF2015] is found in very sandy soils and on
1014 dune systems, whereas *M. reburrus* [JF2015] prefers arid grasslands. Without additional distributional or
1015 host plant data for *M. ampullaceus* [JF2018], we cannot assess whether the single documented locality

1016 for this species represents the center or edge of its range. However, this locality does overlap with the
1017 known range of its sister clade, suggesting that the divergence of *M. ampullaceus* [JF2018] from the *M.*
1018 *aeriballus*–*M. ampullaceus* clade [JF2018] was not a vicariance event.

1019 ***Minyomerus franko* [JF2018]**

1020 *Minyomerus franko* [JF2018] is sister to the *M. caseyi*–*M. trisetosus* clade [JF2015]. The *M. caseyi*–*M.*
1021 *franko* clade [JF2018] (bsv = 4, rfd = 63) is supported by a single synapomorphy and two homoplasious
1022 characters: (1) rows of setae on elytral intervals comprised of larger white setae randomly interspersed
1023 among smaller brown setae(char. 4: 1 – synapomorphic); (2) prementum lacking strong ligula and
1024 straight margins, not appearing pentagonal (char. 7: 0 – homoplasious); and (3) anterior margin of female
1025 tergum VII entirely free of sclerotized band (char. 41: 1 – homoplasious). In addition to these characters,
1026 members of this clade share a generally similar gestalt, especially regarding the head and rostrum, and the
1027 articulation between the pronotum and elytra in dorsal and lateral view. The interspersed, white elytral
1028 setae of these three species exhibit varying degrees of apical expansion, and can appear moderately to
1029 greatly explanate or spatulate in at least some, but not all, specimens.

1030 *Minyomerus franko* [JF2018] has been documented on spear globemallow *Sphaeralcea hastulata*
1031 [non-focal]. *Minyomerus trisetosus* [JF2015] is associated with broomweed *Xanthocephalum* [non-focal],
1032 creosote bush *Larrea tridentata* [non-focal] and snakeweed *Gutierrezia* [non-focal]. *Minyomerus caseyi*
1033 has no known plant associations. It is therefore possible that the divergence of *M. franko* [2018] was
1034 facilitated by differences in host-plant preference. However, this remains unlikely given the generalist
1035 feeding habits of congeners.

1036 Alternatively, the speciation sequence in the *M. caseyi*–*M. franko* clade [JF2018] may correspond to
1037 vicariance events. *Minyomerus trisetosus* [JF2015] inhabits a broad swath of the northern Chihuahuan
1038 Desert, whereas *M. franko* [JF2018] and *M. caseyi* [JF2015] are exclusively encountered in the southern
1039 Chihuahuan Desert. MaxEnt predicts overlapping species distributions for the latter two species. However,
1040 the *documented* localities of these two species pertain to distinct biogeographic regions. *Minyomerus*
1041 *franko* [JF2018] has only been collected in the valleys of the Sierra Madre Oriental range, whereas
1042 *M. caseyi* [JF2015] is found along the western edge of this range, in the eastern portion of the Central
1043 Mexican Plateau. Additional occurrence records are needed to clarify the spatial extents of these species'
1044 distributions, and thus draw more robust inferences regarding their endemism.

1045 **CONCLUSIONS**

1046 Through addition of four herein described species, the entimine [non-focal] genus *Minyomerus* [JF2018]
1047 is expanded to include 21 species. We predict that additional undescribed species of *Minyomerus* [JF2018]
1048 exist throughout the North American deserts, given the narrow endemicity patterns of many members
1049 of the genus. Furthermore, we believe that sampling in poorly-sampled locales, particularly in the
1050 northwestern United States and in northern Mexico, will yield new evolutionary insights for this group.
1051 New molecular data can strengthen phylogenetic hypotheses and provide estimates regarding the timing
1052 of diversification of *Minyomerus* [JF2018], thereby testing our current inference of an origin in central
1053 Mexico. Another research direction should focus on the reproductive behavior of certain species suspected
1054 to be parthenogenetic; including rearing and karyotyping. Finally, the validity of the genus *Minyomerus*
1055 [JF2018] as a member of the Tanymecini [non-focal], and its relationships to other Entiminae [non-focal],
1056 remain uncertain.

1057 **ACKNOWLEDGMENTS**

1058 The authors are grateful to Robert Anderson (CMNC), Ed Riley and John Oswald (TAMU), and Lourdes
1059 Chamorro (USNM) for their assistance and provision of specimens used in this revision. The authors also
1060 thank Salvatore Anzaldo, Andrew Johnston, Sangmi Lee and other ASUHIC members for their assistance
1061 in procuring, treating, and maintaining specimen loans upon entry into the ASUHIC. This research was
1062 funded in part by the National Science Foundation (DEB-1155984) and the United States Department of
1063 Agriculture – Agricultural Research Service (Agreement 58-1275-1-335).

1064 **SUPPLEMENTAL INFORMATION**

1065 **SI1** Explanation of the RCC–5 alignment approach. File format: .pdf

1066 **SI2A** Input constraints for the *Minyomerus* [JF2018]/[JF2015] rank-only classification alignment. File
1067 format: .txt
1068 **SI2B** Input visualization for the SI2A input. File format: .pdf
1069 **SI2C** Set of 114 *Maximally Informative Relations* (MIR) for the SI2A input. File format: .csv
1070 **SI2D** Alignment visualization for the SI2A input. File format: .pdf
1071 **SI3A** Input constraints for the *Minyomerus* [JF2018]/[JF2015] phylogeny alignment – whole-concept
1072 resolution with overlap. File format: .txt
1073 **SI3B** Input visualization for the SI3A input. File format: .pdf
1074 **SI3C** Set of 925 *Maximally Informative Relations* (MIR) for the SI3A input. File format: .csv
1075 **SI3D** Alignment visualization for the SI3A input. File format: .pdf
1076 **SI4A** Input constraints for the *Minyomerus* [JF2018]/[JF2015] phylogeny alignment – split-concept
1077 resolution. File format: .txt
1078 **SI4B** Input visualization for the SI4A input. File format: .pdf
1079 **SI4C** Set of 925 *Maximally Informative Relations* (MIR) for the SI4A input. File format: .csv
1080 **SI4D** Alignment visualization for the SI4A input. File format: .pdf

1081 REFERENCES

- 1082 Agnarsson, I. & Miller, J. A. (2008), 'Is ACCTRAN better than DELTRAN?', *Cladistics* **24**(6), 1032–
1083 1038.
- 1084 Alonso-Zarazaga, M. A. & Lyal, C. H. C. (1999), *A world catalogue of families and genera of Cur-*
1085 *culionoidea (Insecta: Coleoptera)*, Entomopraxis, Barcelona, Spain.
- 1086 Anderson, R. S. (2002), Curculionidae, in R. H. Arnett Jr., M. C. Thomas, P. E. Skelley & J. H. Frank,
1087 eds, 'American Beetles, Volume 2, Polyphaga: Scarabaeoidea to Curculionoidea', CRC Press, Boca
1088 Raton, FL, chapter 131, p. 722–815.
- 1089 Arnett Jr., R. H., Samuelson, G. A., Nishida, G. M. et al. (1993), *The insect and spider collections of the*
1090 *world*., 2 edn, Sandhill Crane Press, Inc., Gainesville, Florida.
- 1091 Blackwelder, R. E. & Blackwelder, R. M. (1948), *Fifth Supplement, 1939 to 1947 (Inclusive) to the Leng*
1092 *Catalogue of Coleoptera of America, North of Mexico*, Mount Vernon, Virginia.
- 1093 Boheman, C. H. (1833), 12. T. Microsus, in C. J. Schoenherr, ed., 'Genera et species curculionidum, cum
1094 synonymia hujus familiae', Vol. 1:2, Nicolas-Edme Roret, Paris, France, pp. 523–524.
- 1095 Bouchard, P., Bousquet, Y., Davies, A. E., Alonso-Zarazaga, M. A., Lawrence, J. F., Lyal, C. H., Newton,
1096 A. F., Reid, C. A., Schmitt, M., Ślipiński, S. A. et al. (2011), 'Family-group names in Coleoptera
1097 (Insecta)', *ZooKeys* **88**, 1–972.
- 1098 Bremer, K. A. et al. (1994), 'Branch support and tree stability', *Cladistics* **10**(3), 295–304.
- 1099 Brown, R. W. (1956), *Composition of scientific words*, Smithsonian Institution Press, Washington, DC.
- 1100 Casey, T. L. (1889), 'On some new north american rhynchophora', *Annals of the New York Academy of*
1101 *Sciences* **4**(1), 229–296.
- 1102 Chen, M., Yu, S., Franz, N., Bowers, S. & Ludäscher, B. (2014), 'Euler/x: A toolkit for logic-based
1103 taxonomy integration', *arXiv* **1402**(1992), 1–8.
- 1104 de la Torre-Bueno, J. R., Nichols, S. W., Tulloch, G. S., de la Torre-Bueno, J. R. et al. (1989), *Torre-Bueno*
1105 *glossary of entomology*, New York Entomological Society in cooperation with the American Museum
1106 of Natural History, New York City, New York.
- 1107 Elith, J., Phillips, S. J., Hastie, T., Dudík, M., Chee, Y. E. & Yates, C. J. (2011), 'A statistical explanation
1108 of MaxEnt for ecologists', *Diversity and distributions* **17**(1), 43–57.
- 1109 Farris, J. S. (1989), 'The retention index and the rescaled consistency index', *Cladistics* **5**(4), 417–419.
- 1110 Franz, N. M. (2010a), 'Redescriptions of critical type species in the *Eustylini* Lacordaire (Coleoptera:
1111 Curculionidae: Entiminae)', *Journal of Natural History* **44**(1–2), 41–80.
- 1112 Franz, N. M. (2010b), 'Revision and phylogeny of the Caribbean weevil genus *Apotomoderes* Dejean,
1113 1834 (Coleoptera, Curculionidae, Entiminae).', *ZooKeys* **49**.
- 1114 Franz, N. M. (2012), 'Phylogenetic reassessment of the *Exophthalmus* genus complex (Curculionidae:
1115 Entiminae: Eustylini, Geonemini)', *Zoological Journal of the Linnean Society* **164**(3), 510–557.
- 1116 Franz, N. M. (2014), 'Anatomy of a cladistic analysis', *Cladistics* **30**(3), 294–321.
- 1117 Franz, N. M., Chen, M., Kianmajd, P., Yu, S., Bowers, S., Weakley, A. S. & Ludäscher, B. (2016b),
1118 'Names are not good enough: Reasoning over taxonomic change in the andropogon complex', *Semantic*
1119 *Web (IOS)* **7**(6), 645–667.
- 1120 Franz, N. M., Musher, L. J., Brown, J. W., Yu, S., hen, M., Yu, S. & Ludäscher, B. (2018), 'Verbalizing
1121 phylogenomic conflict: Representation of node congruence across competing reconstructions of the
1122 neoavian explosion', *bioRxiv* pp. 1–52. <https://doi.org/10.1101/233973>.
- 1123 Franz, N. M. & Peet, R. K. (2009), 'Towards a language for mapping relationships among taxonomic
1124 concepts', *Systematics and Biodiversity* **7**(1), 5–20.
- 1125 Franz, N. M., Pier, N. M., Reeder, D. M., Chen, M., Yu, S., Kianmajd, P., Bowers, S. & Ludäscher, B.
1126 (2016a), 'Two influential primate classifications logically aligned', *Systematic Biology* **65**(4), 561–582.
- 1127 Goloboff, P. A. (1999), *NONA - Version 2.0 (for Windows)*. <http://www.cladistics.com>.
- 1128 Goloboff, P. A. & Farris, J. S. (2001), 'Methods for quick consensus estimation', *Cladistics* **17**(1), S26–
1129 S34.
- 1130 Goloboff, P. A., Farris, J. S. & Nixon, K. C. (2008), 'Tnt, a free program for phylogenetic analysis',
1131 *Cladistics* **24**(5), 774–786.
- 1132 Google Inc. (2018), *Google Earth Pro - Version 7.3.1.4507*. <https://www.google.com/earth/>.
- 1133 Green, J. W. (1920), 'Notes on American Rhynchophora (Col.)', *Entomological News* **31**, 193–201.
- 1134 Hijmans, R. J., Cameron, S. E., Parra, J. L., Jones, P. G. & Jarvis, A. (2005), 'Very high resolution
1135 interpolated climate surfaces for global land areas', *International journal of climatology* **25**(15), 1965–

- 1136 1978.
- 1137 Hijmans, R. J., Garcia, N., Kapoor, J., Rala, A., Maunahan, A. & Wieczorek, J. (2012), *Global administrative areas (boundaries)*, Museum of Vertebrate Zoology and the International Rice Research Institute, University of California, Berkeley, California. <http://www.gadm.org/>.
- 1138
- 1139
- 1140 Horn, G. H. (1876), Family V. OTIORHYNCHIDÆ, in J. L. LeConte & G. H. Horn, eds, 'The Rhynchophora of America, north of Mexico', Vol. 15, Proceedings of the American Philosophical Society, New York City, New York, pp. 13–112.
- 1141
- 1142
- 1143 Howden, A. T. (1959), 'A revision of the species of *Pandeleteius* Schönherr and *Pandeleteinus* Champion of America north of Mexico: (Coleoptera: Curculionidae)', *Proceedings of the California Academy of Sciences* **29**, 361–421.
- 1144
- 1145
- 1146 Howden, A. T. (1970), 'The Tanymecini of the West Indies (Coleoptera: Curculionidae)', *Contributions of the American Entomological Institute* **5**, 1–73.
- 1147
- 1148 Howden, A. T. (1982), 'Revision of the New World genus *Hadromeropsis* Pierce (Coleoptera, Curculionidae, Tanymecini)', *Contributions of the American Entomological Institute* **19**, 1–180.
- 1149
- 1150 Howden, A. T. (1995), 'Structures related to oviposition in Curculionoidea', *Memoirs of the Entomological Society of Washington* **14**, 53–100.
- 1151
- 1152 Jansen, M. A. & Franz, N. M. (2015), 'Phylogenetic revision of *Minyomerus* Horn, 1876 sec. Jansen and Franz, 2015 (Coleoptera: Curculionidae) using taxonomic concept annotations and alignments', *ZooKeys* **528**, 1–133.
- 1153
- 1154
- 1155 Kissinger, D. G. (1964), *Curculionidae of America North of Mexico. A Key to the Genera*, Taxonomic Publications, South Lancaster, Massachusetts.
- 1156
- 1157 LeConte, J. L. (1859), *The Complete Writings of Thomas Say on the Entomology of North America*, Baillière Brothers, London, England.
- 1158
- 1159 LeConte, J. L. & Horn, G. H. (1876), 'The Rhynchophora of America, north of Mexico', *Proceedings of the American Philosophical Society* **15**(96), 1–455.
- 1160
- 1161 Marvaldi, A. E. (1997), 'Higher level phylogeny of Curculionidae (Coleoptera: Curculionoidea) based mainly on larval characters, with special reference to broad-nosed weevils', *Cladistics* **13**(4), 285–312.
- 1162
- 1163 Marvaldi, A. E., Lanteri, A. A., del Río, M. G. & Oberprieler, R. G. (2014), Entiminae Schoenherr, 1823, in R. A. B. Leschen & R. G. Beutel, eds, 'Handbook of Zoology: Arthropoda: Insecta: Coleoptera Volume 3: Morphology and Systematics (Phytophaga)', De Gruyter, Berlin, Germany, chapter 3.7.5, p. 503–522.
- 1164
- 1165
- 1166
- 1167 Morimoto, K. & Kojima, H. (2003), 'Morphologic characters of the weevil head and phylogenetic implications (Coleoptera, Curculionoidea)', *Esakia* **43**, 133–169.
- 1168
- 1169 Munz, P. A. & Keck, D. D. (1973), *A Californian flora (with supplement)*, University of California Press, Berkeley, California.
- 1170
- 1171 Nixon, K. C. & Carpenter, J. M. (1993), 'On outgroups', *Cladistics* **9**(4), 413–426.
- 1172 Nixon, K. C. et al. (2002), *WinClada - Version 1.00. 08*. <http://www.diversityoflife.org/winclada/>.
- 1173 Oberprieler, R. G., Anderson, R. S. & Marvaldi, A. E. (2014), Curculionoidea Latreille, 1802: Introduction, Phylogeny, in R. A. B. Leschen & R. G. Beutel, eds, 'Handbook of Zoology: Arthropoda: Insecta: Coleoptera Volume 3: Morphology and Systematics (Phytophaga)', De Gruyter, Berlin, Germany, chapter 3, pp. 285–300.
- 1174
- 1175
- 1176
- 1177 Oberprieler, R. G., Marvaldi, A. E. & Anderson, R. S. (2007), 'Weevils, weevils, weevils everywhere', *Zootaxa* **1668**(1), 491–520.
- 1178
- 1179 O'Brien, C. W. & Wibmer, G. J. (1982), *Annotated checklist of the weevils (Curculionidae sensu lato) of North America, Central America, and the West Indies (Coleoptera: Curculionoidea)*, American Entomological Institute, Ann Arbor, Michigan.
- 1180
- 1181
- 1182 Phillips, S. J., Anderson, R. P. & Schapire, R. E. (2006), 'Maximum entropy modeling of species geographic distributions', *Ecological modelling* **190**(3–4), 231–259.
- 1183
- 1184 Phillips, S. J., Dudík, M. & Schapire, R. E. (2004), A maximum entropy approach to species distribution modeling, in 'Proceedings of the 21st International Conference on Machine Learning', ACM, pp. 83–90.
- 1185
- 1186 Pierce, W. D. (1909), 'Studies of North American weevils', *Proceedings of the United States National Museum* **37**(1708), 325–364.
- 1187
- 1188 Pierce, W. D. (1913), 'Miscellaneous contributions to the knowledge of the weevils of the families Attelabidae and Brachyrhinidae', *Proceedings of the United States National Museum* **45**(1988), 365–426.
- 1189
- 1190

- 1191 Quantum GIS Development Team (2018), ‘Quantum GIS Geographic Information System’, *Open Source*
1192 *Geospatial Foundation Project*. <http://qgis.osgeo.org>.
- 1193 Rieppel, O. (2007), ‘The performance of morphological characters in broad-scale phylogenetic analyses’,
1194 *Biological Journal of the Linnean Society* **92**(2), 297–308.
- 1195 Say, T. (1831), Descriptions of North American Curculionides and an arrangement of some of our known
1196 species agreeably to the method of Schoenherr, *in* J. L. LeConte, ed., ‘The Complete Writings of
1197 Thomas Say on the Entomology of North America’, Vol. 1, Baillière Brothers, London, England,
1198 pp. 1–30.
- 1199 SEINet (2018), *Southwest Environmental Information Network*. <http://swbiodiversity.org/seinet/index.php>.
- 1200 Sharp, D. (1891), Coleoptera. Rhynchophora. Curculionidae. Attelabinae, Pterocolinae, Allocoryninae,
1201 Apioninae, Thecesterninae, Otiorhynchinae [part, “Apterae”], *in* D. Sharp & G. C. Champion, eds,
1202 ‘Biologia Centrali-Americanana’, Vol. 4:3, London, England, pp. 87–177.
- 1203 Sleeper, E. L. (1960), ‘Notes on the Curculionoidea II: 20. a contribution to the knowledge of the
1204 Curculionoidea’, *Ohio Journal of Science* **60**(2), 83–88.
- 1205 Thompson, R. T. (1992), ‘Observations on the morphology and classification of weevils (Coleoptera,
1206 Curculionoidea) with a key to major groups’, *Journal of Natural History* **26**(4), 835–891.
- 1207 Ting, P. C. (1936), ‘The mouth parts of the coleopterous group Rhynchophora’, *Microentomology*
1208 **1**, 93–114.
- 1209 Wheeler, Q. D. & Platnick, N. I. (2000), The phylogenetic species concept (*sensu* Wheeler and Platnick),
1210 *in* Q. D. Wheeler & R. Meier, eds, ‘Species Concepts and Phylogenetic Theory: a Debate’, Columbia
1211 University Press, New York City, New York, pp. 55–69.
- 1212 Wilson, J. S. & Pitts, J. P. (2010), ‘Illuminating the lack of consensus among descriptions of earth
1213 history data in the north american deserts: a resource for biologists’, *Progress in Physical Geography*
1214 **34**(4), 419–441.



Figure 1. Dorsal habitus of *M. ampullaceus* [JF2018]. Image of female (♀) holotype.



Figure 2. Lateral habitus of *M. ampullaceus* [JF2018]. Image of female (♀) holotype.



Figure 3. Ventral habitus of *M. ampullaceus* [JF2018]. Image of female (♀) holotype.



Figure 4. Head and rostrum of *M. ampullaceus* [JF2018]. Frontal view of female (♀) holotype.



Figure 5. Spermatheca of *M. ampullaceus* [JF2018]. Genitalia of female (♀) holotype.



Figure 6. Lamina of spiculum ventrale of *M. ampullaceus* [JF2018]. Sternum VIII of female (♀) holotype.



Figure 7. Dorsal habitus of *M. franko* [JF2018]. Image of female (♀) holotype.



Figure 8. Lateral habitus of *M. franko* [JF2018]. Image of female (♀) holotype.



Figure 9. Ventral habitus of *M. franko* [JF2018]. Image of female (♀) holotype.



Figure 10. Head and rostrum of *M. franko* [JF2018]. Frontal view of female (♀) holotype.



Figure 11. Maxilla of *M. franko* [JF2018]. Dextral maxilla of female (♀) paratype.



Figure 12. Prementum of *M. franko* [JF2018]. Labium of female (♀) paratype.



Figure 13. Spermatheca of *M. franko* [JF2018]. Genitalia of female (♀) paratype.

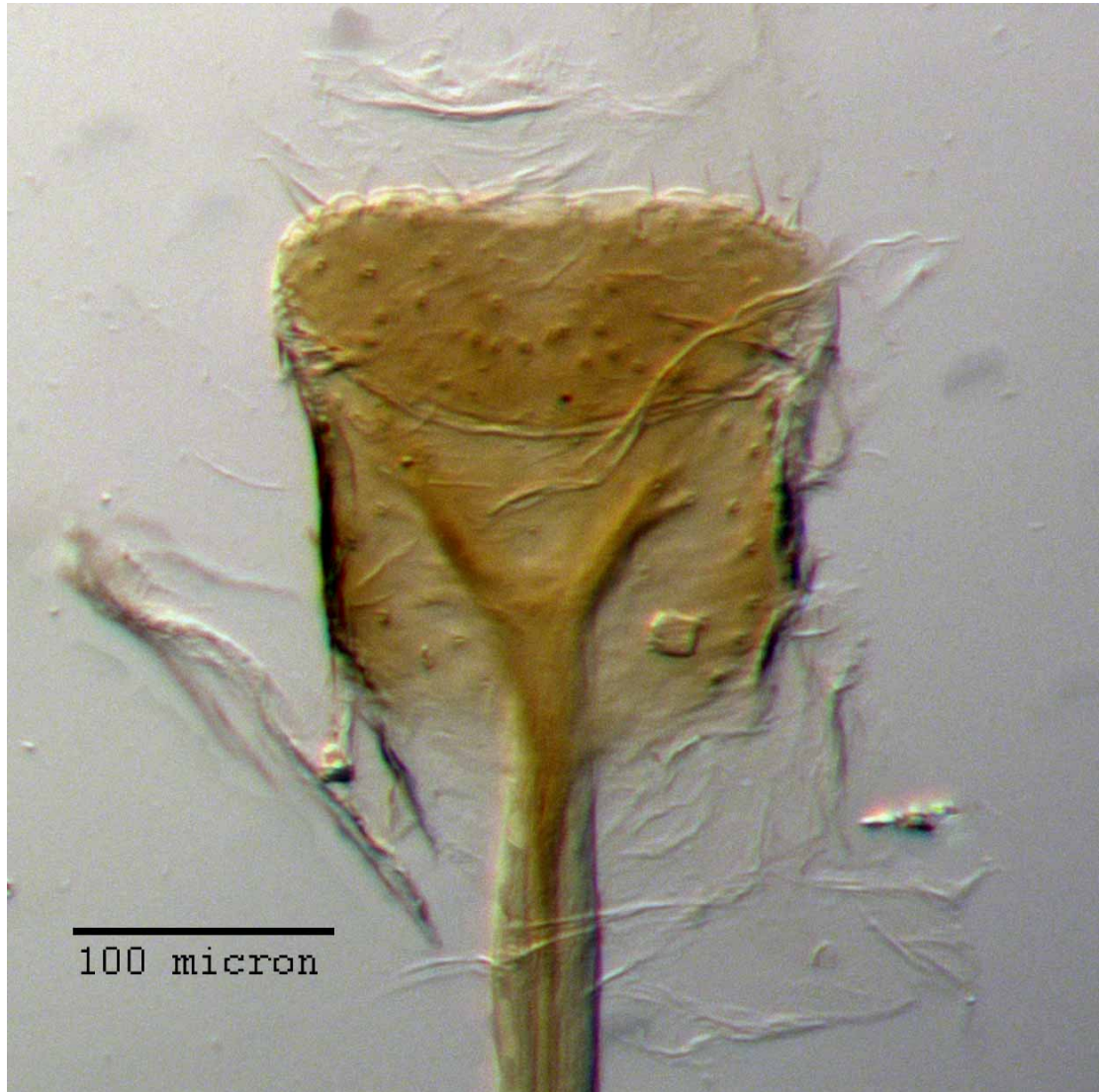


Figure 14. Lamina of spiculum ventrale of *M. franko* [JF2018]. Sternum VIII of female (♀) paratype.



Figure 15. Aedeagus of *M. franko* [JF2018]. Genitalia of male (σ) paratype in (A) dorsal view and (B) lateral view.



Figure 16. Dorsal habitus of *M. sculptilis* [JF2018]. Image of female (♀) holotype.



Figure 17. Lateral habitus of *M. sculptilis* [JF2018]. Image of female (♀) holotype.



Figure 18. Ventral habitus of *M. sculptilis* [JF2018]. Image of female (♀) holotype.



Figure 19. Head and rostrum of *M. sculptilis* [JF2018]. Frontal view of female (♀) holotype.

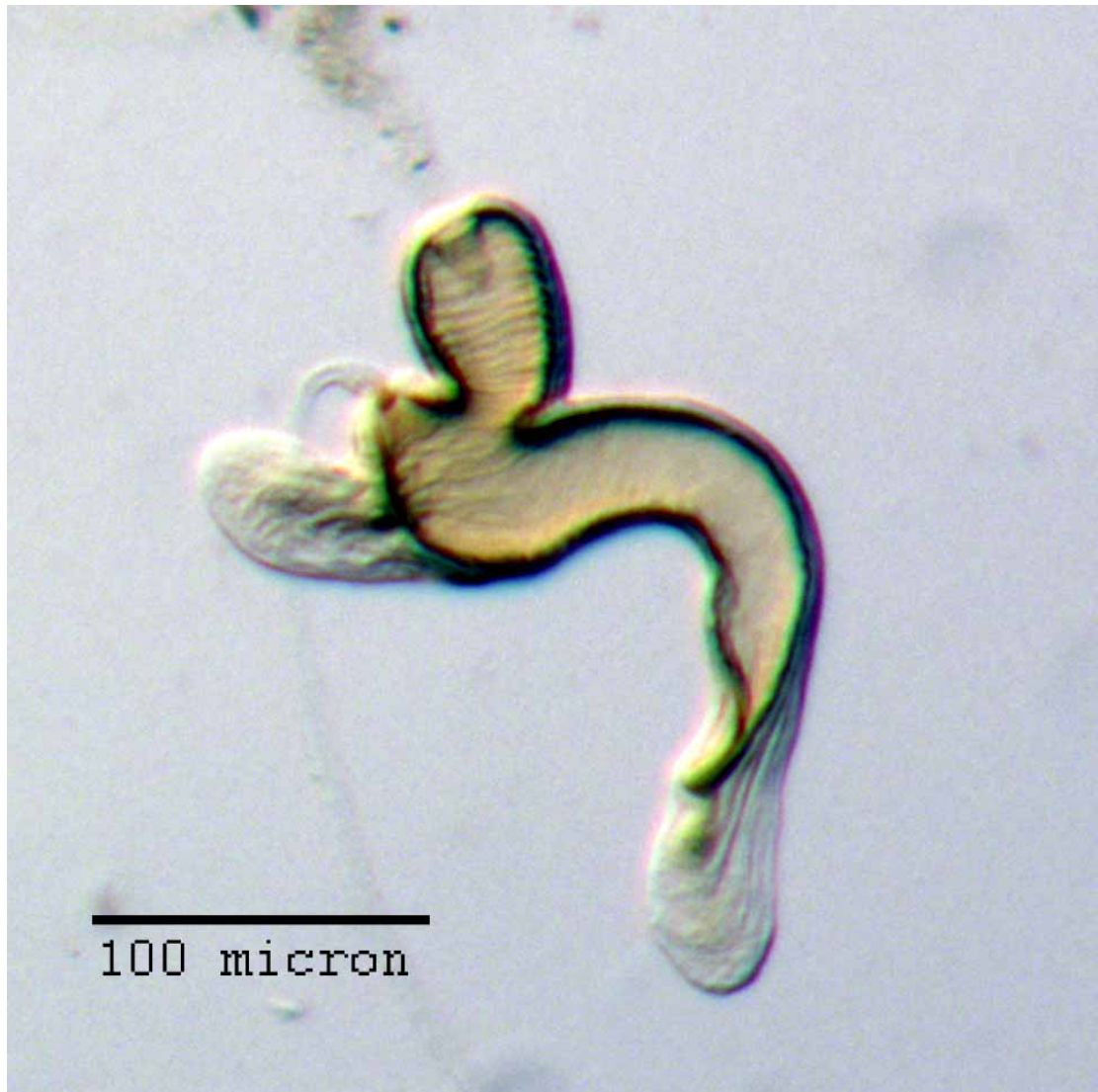


Figure 20. Spermatheca of *M. sculptilis* [JF2018]. Genitalia of female (♀) paratype.

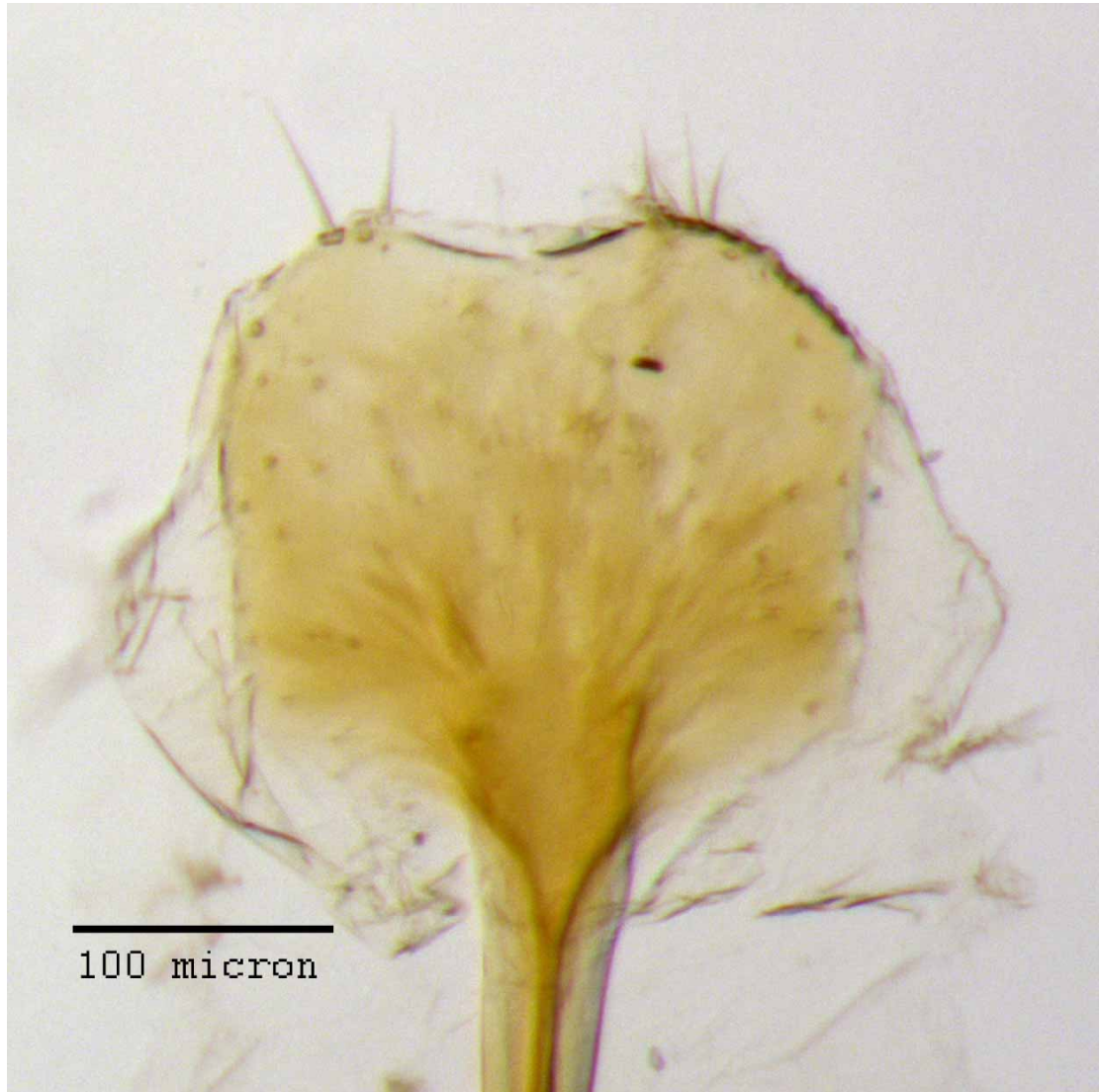


Figure 21. Lamina of spiculum ventrale of *M. sculptilis* [JF2018]. Sternum VIII of female (♀) paratype.



Figure 22. Aedeagus of *M. sculptilis* [JF2018]. Genitalia of male (σ) paratype in (A) dorsal view and (B) lateral view.



Figure 23. Dorsal habitus of *M. tylotos* [JF2018]. Image of female (♀) holotype.



Figure 24. Lateral habitus of *M. tylotos* [JF2018]. Image of female (♀) holotype.



Figure 25. Ventral habitus of *M. tylotos* [JF2018]. Image of female (♀) holotype.



Figure 26. Head and rostrum of *M. tylotos* [JF2018]. Frontal view of female (♀) holotype.

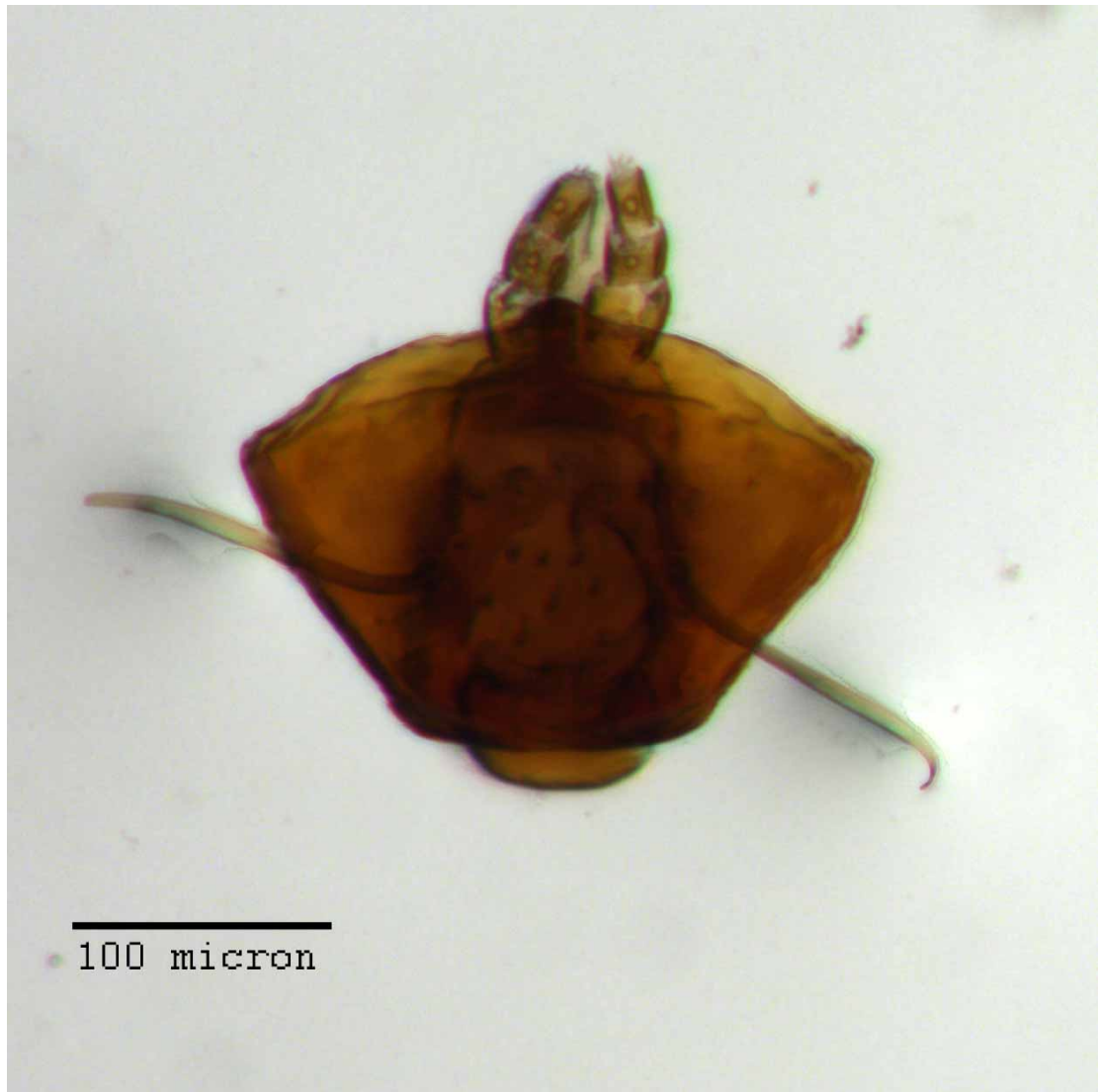


Figure 27. Prementum of *M. tylotos* [JF2018]. Labium of female (♀) paratype.



Figure 28. Spermatheca of *M. tylotos* [JF2018]. Genitalia of female (♀) paratype.



Figure 29. Lamina of spiculum ventrale of *M. tylotos* [JF2018]. Sternum VIII of female (♀) paratype.

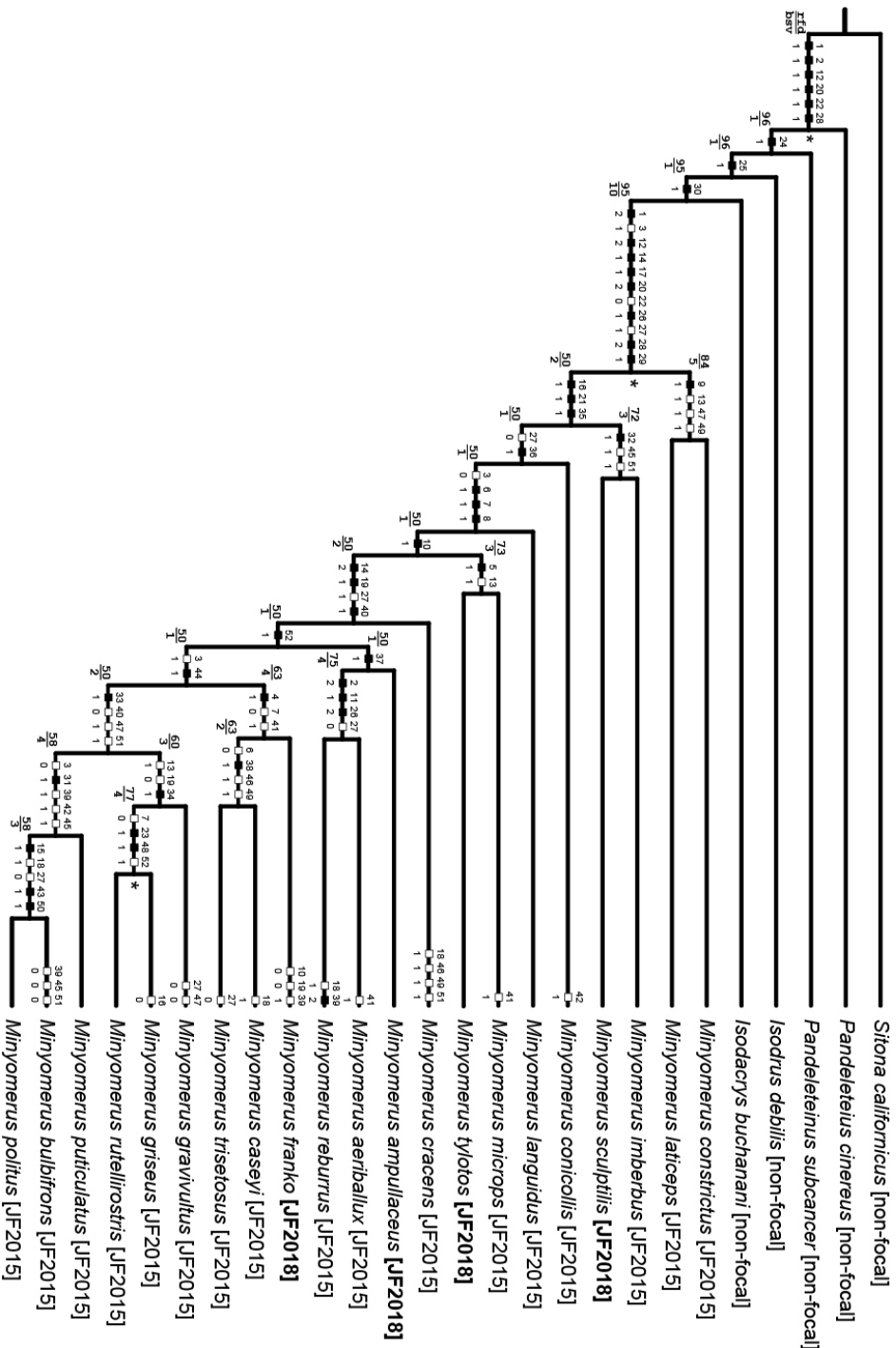


Figure 30. Preferred phylogeny – character transitions and support. Single most parsimonious cladogram representing the preferred phylogeny of species of *Minyomerus* [JF2018], and select outgroup taxa ($L = 99$, $CI = 60$, $RI = 80$). Characters 9, 27, 39, 45 - 47, 49, and 51 are mapped under ACCTRAN optimization; all others are unambiguously optimized. Black squares indicate non-homoplasious character state changes, whereas white squares indicate homoplasious character state changes. The numbers above and below the squares represent character numbers and states, respectively. Bremer support (upper value) and relative fit difference (lower value) values can be found at the left ends of the branches. A "*" symbol at the right end of a branch indicates Bootstrap support greater than 0.95.

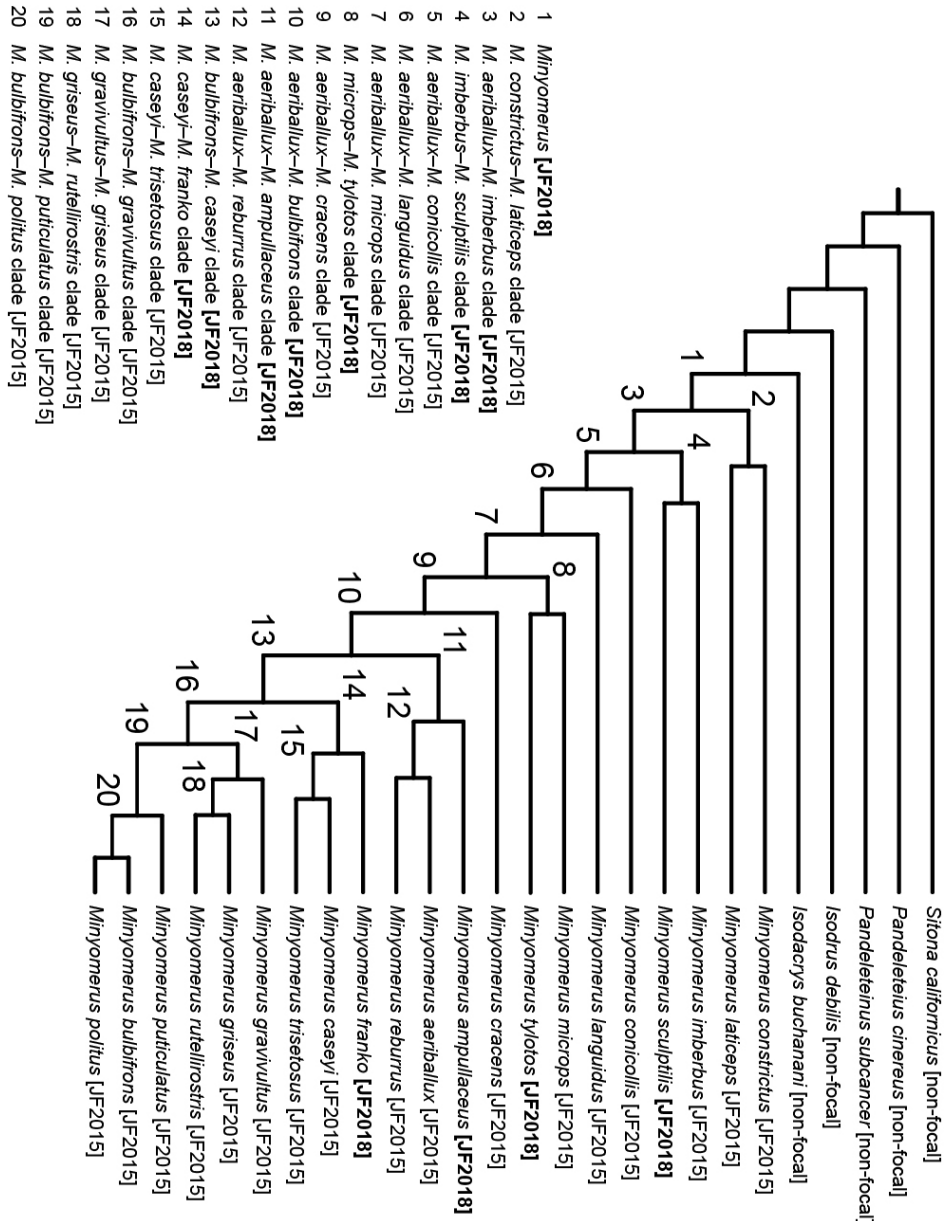


Figure 31. Preferred phylogeny – clade concept labels. Topology and species-level taxonomic concept labels as in Fig. 30. Clade concept labels, numbered 1-20, are consistently generated by using the alphabetically first epithet in each of the bifurcating sister clades. This method safeguards the clade concept labels against changes due simply to reorientation of leaves. Bold-font square brackets indicate new [JF2018] labels. See also **RCC-5 Alignments**.

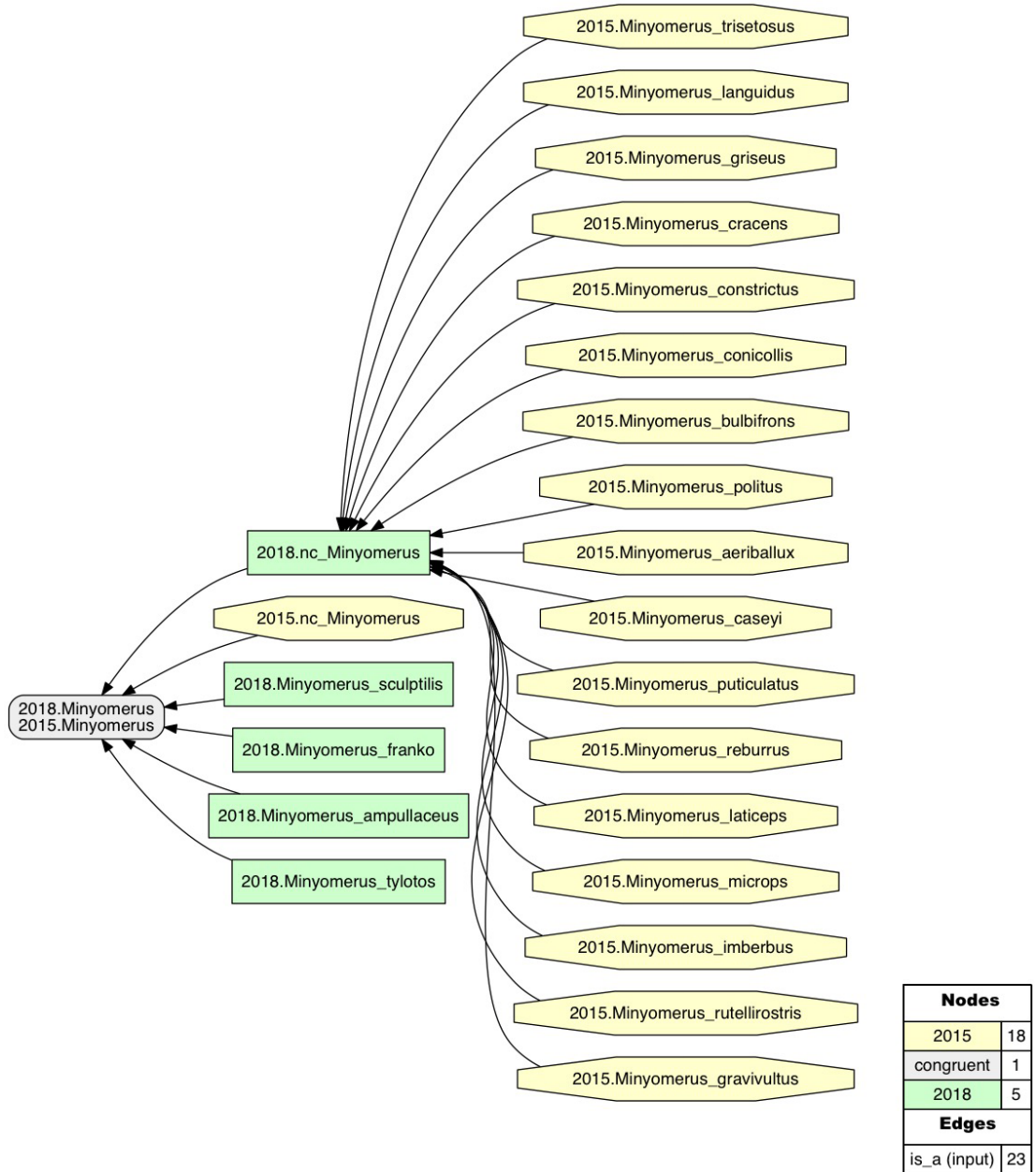


Figure 32. Intensional RCC-5 alignment of the rank-only classifications of *Minyomerus* [JF2018]/[JF2015]. See also Jansen & Franz (2015) and Supplemental Information SI2. Taxonomic concept labels such as *Minyomerus microps* [JF2015] are abbreviated as "2015.Minyomerus_microps". Relaxation of the coverage constraint is indicated with the prefix "nc_" (no coverage). Congruent concept regions (T_2 and T_1) are shown as grey rectangles, concepts regions unique to the later taxonomy (T_2) are shown as green rectangles, and concept regions unique to the earlier taxonomy (T_1) are shown as yellow octagons. Articulations of inverse proper inclusion (<) and overlap (><), where present, are also shown.

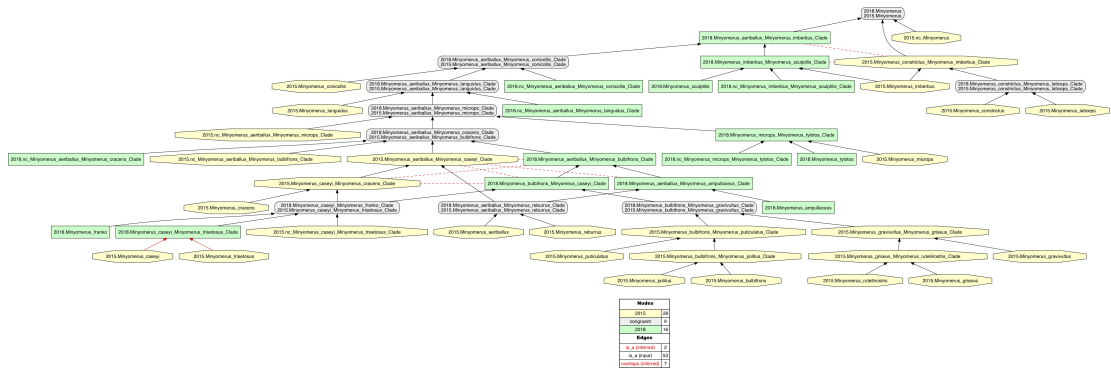


Figure 33. Intensional RCC–5 alignment of the phylogenies of *Minyomerus* [JF2018]/[JF2015] – whole-concept resolution with overlap. See also **Supplemental Information SI3**. Seven overlapping articulations are inferred. For further discussion, see the **RCC–5 Alignments** section.

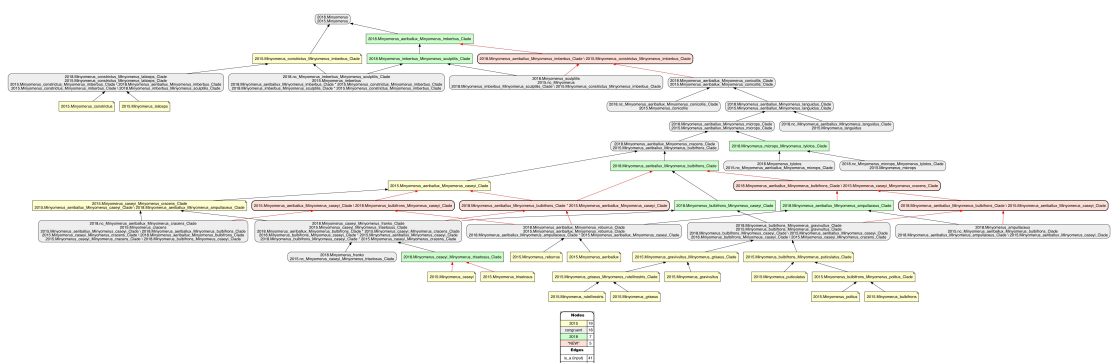


Figure 34. Intensional RCC–5 alignment of the phylogenies of *Minyomerus* [JF2018]/[JF2015] – split-concept resolution. See also **Supplemental Information SI4**. The seven overlapping articulations of the alignment displayed Fig. 33 are resolved into their constituent split regions. That is, if regions A and B overlap, the three resulting split regions are labeled A\|b ("A, not b"), A*B ("A and B"), and B\|a ("B, not a"). Five split-concept regions can *only* be named using this convention, and are salmon-colored in the alignment visualization.

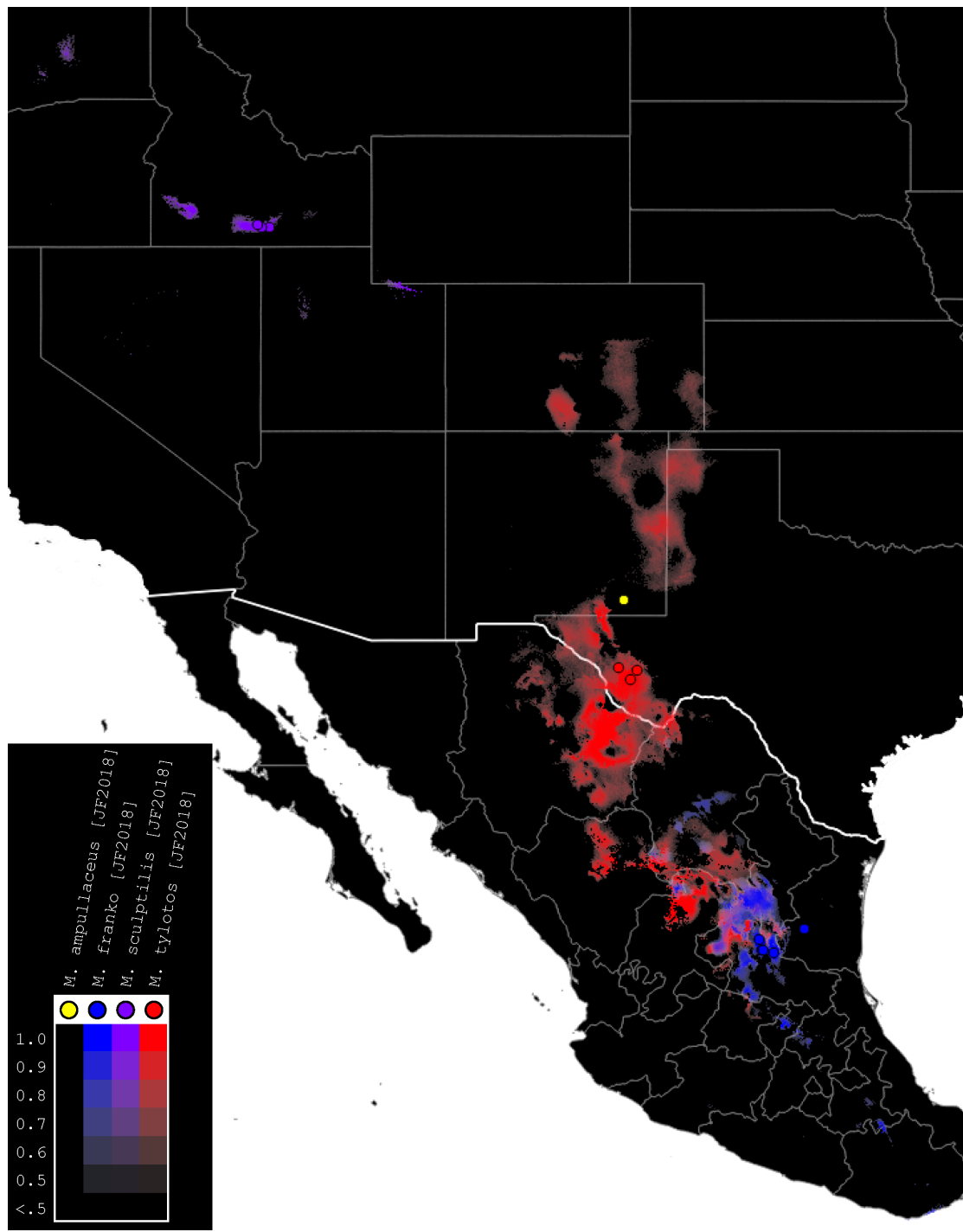


Figure 35. Summary map of distributions of new species of *Minyomerus* [JF2018]. Combined occurrence record and Maxent habitat modeling map for four newly-described species of *Minyomerus* [JF2018], as indicated in the legend.

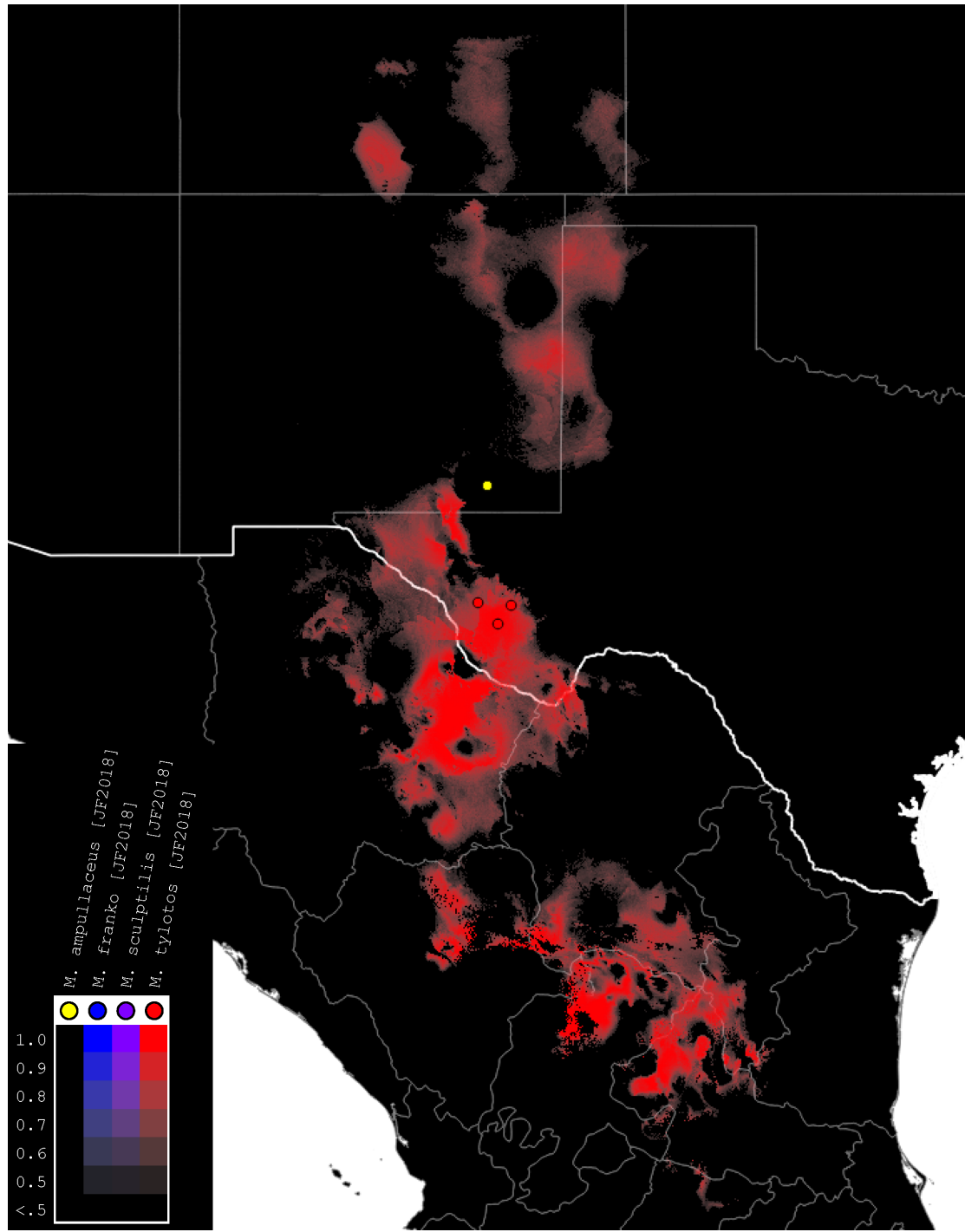


Figure 36. Distributions of *M. ampullaceus* [JF2018] and *M. tylotos* [JF2018]. Combined occurrence record and Maxent habitat modeling map for *M. ampullaceus* [JF2018] and *M. tylotos* [JF2018], as indicated in the legend.

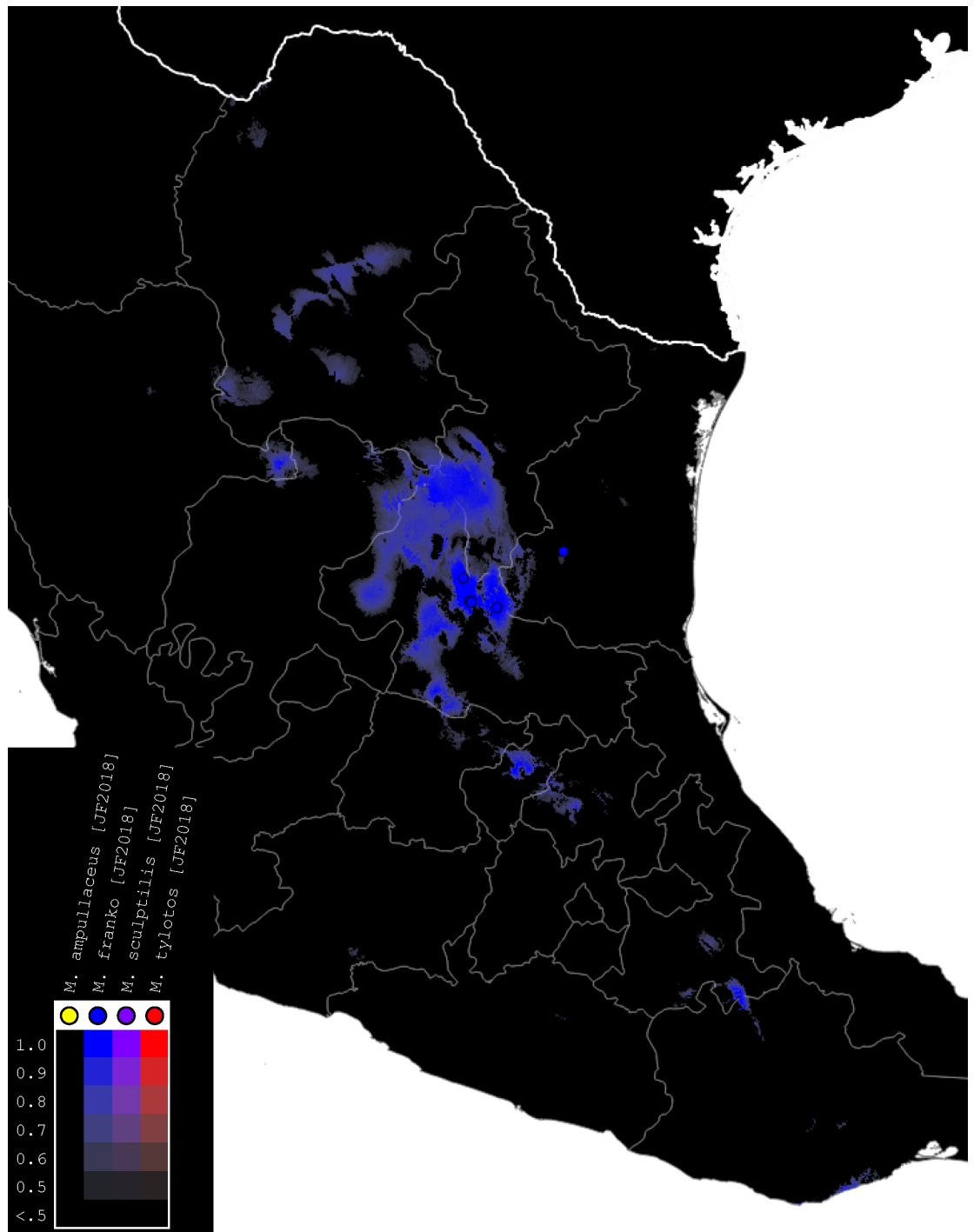


Figure 37. Distributions of *M. franko* [JF2018]. Combined occurrence record and Maxent habitat modeling map for *M. franko* [JF2018], as indicated in the legend.

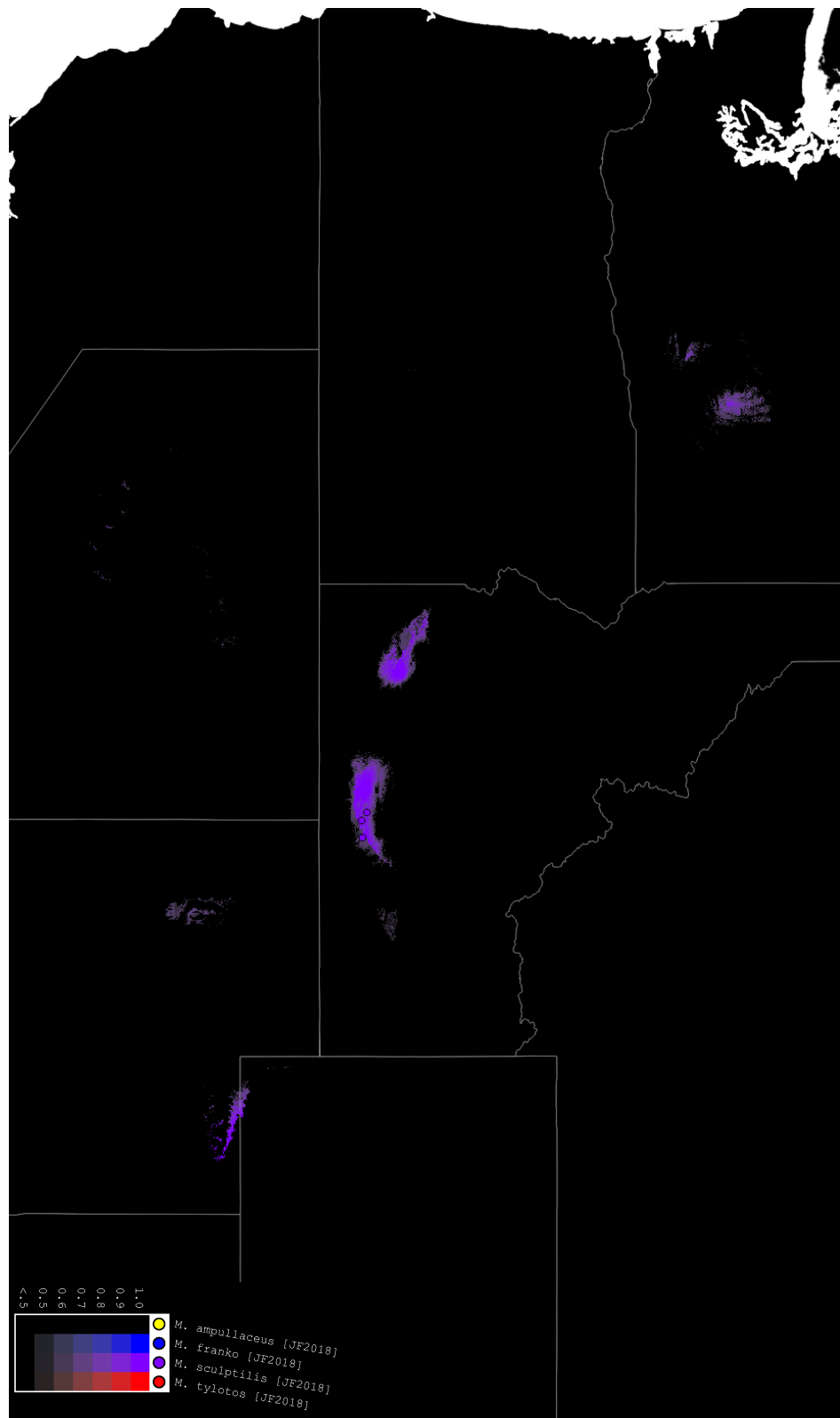


Figure 38. Distributions of *M. sculptilis* [JF2018]. Combined occurrence record and Maxent habitat modeling map for *M. sculptilis* [JF2018], as indicated in the legend.